Effect of Marangoni stress on the bulk rheology of a dilute emulsion of surfactant-laden deformable droplets in linear flows

Shubhadeep Mandal, Sayan Das, and Suman Chakraborty*
Department of Mechanical Engineering, Indian Institute of Technology Kharagpur, West Bengal-721302, India
(Received 24 May 2017; published 17 November 2017)

In the present study, we analytically investigate the deformation and bulk rheology of a dilute emulsion of surfactant-laden droplets suspended in linear flows. We use an asymptotic approach to determine the effect of surfactant distribution on the deformation of an isolated droplet as well as the effective shear and extensional viscosity for a dilute emulsion. The nonuniform distribution of surfactants due to the bulk flow results in the generation of a Marangoni stress, which affects both the deformation as well as the bulk rheology of the emulsion. The present analysis is done for the limiting case when the surfactant transport is dominated by the surface diffusion relative to surface convection. As an example, we have used two commonly encountered bulk flows, namely, uniaxial extensional flow and simple shear flow. With the assumption of negligible inertial forces present in either of the phases, we show that both the surfactant concentration on the droplet surface as well as the ratio of viscosity of the droplet phase with respect to the suspending fluid has a significant effect on the droplet deformation as well as the bulk rheology. It is seen that increase in the nonuniformity in surfactant distribution on the droplet surface results in a higher droplet deformation and a higher effective viscosity for either of the linear flows considered. The effect of surfactant distribution on effective viscosity is insignificant for highly viscous droplets. For the case of simple shear flow, surfactant distribution is found to have no effect on the inclination angle. However, a higher viscosity ratio predicts the droplet to be more aligned toward the direction of flow. First and second normal stress differences are present for the case of a simple shear flow, of which the former is found to increase with nonuniformity in surfactant distribution, whereas the later remains unaffected.

DOI: 10.1103/PhysRevFluids.2.113604

I. INTRODUCTION

Emulsions, polymer blends, and foams encompass a longstanding leading area of research because of their wide application in foods, material processing, and pharmaceuticals [1–3]. The droplets of the dispersed phase suspended in a carrier phase are deformed, oriented, and broken up during these processes, resulting in changes in their microstructure or morphology. The modified morphology alters the mechanical, thermal, and chemical properties of the emulsions [1–7]. The dynamics of suspended droplets also finds its wide application in different microfluidic devices [8–10]. Some of the common use of droplets in microfluidic devices can be found in cell encapsulation, reagent mixing, drug delivery, and analytic detection [8,11–14].

Hydrodynamics of clean droplets in linear flows (i.e., extensional and simple shear) has been studied extensively since the classical work of Taylor [15,16]. When the flow strength is relatively small as compared to the interfacial tension, a droplet deforms into an ellipsoidal shape. In uniaxial extensional flow, the ellipsoidal droplet is aligned with the extension axis, while the ellipsoidal droplet makes an angle with the flow direction in simple shear flow (refer to Stone [17] for detail review). Presence of droplets perturbs the imposed flow and thereby alters the bulk rheology of the emulsion. Theoretical studies have predicted increase in both the extensional and shear viscosities of emulsion.

*suman@mech.iitkgp.ernet.in

In the presence of droplet deformation, a dilute emulsion is found to exhibit non-Newtonian behavior, such as nonzero first and second normal stress differences (refer to Pal [18] for detailed review).

Most of the existing studies have focused on the hydrodynamics of surfactant-free droplet. Toward investigating the dynamics of surfactant-laden droplet, Flumerfelt has performed a perturbation analysis to study the effect of the varying interfacial tension as well as shear and dilatational interfacial viscosity, in the presence of mass transfer, on the deformation of a droplet suspended in linear flows [19]. These interfacial viscosities at the interface are generated due to the presence of contaminants or surfactants on the droplet surface. Later, Stone and Leal [20] have performed analytical and numerical studies and determined the effect of bulk-insoluble surfactants on the droplet deformation. They have performed a small-deformation analysis, considering the limit of diffusion-dominated surfactant transport, and obtained the first correction in droplet shape. For a surfactant-laden droplet, the surface tension varies along the interface of the droplet due to a nonuniform distribution of surfactants along the droplet surface, with lower surface tension in regions of high surfactant concentration. Several experimental studies have shown that there is a close relationship between droplet deformation and local surfactant distribution along the droplet surface [15–25]. Milliken *et al.* [26] numerically investigated the effect of surfactant distribution on the deformation and breakup of a droplet suspended in a uniaxial extensional flow. For the case of an imposed extensional flow, the droplet elongates and there is a higher concentration of surfactants and hence a lower surface tension at the two tips of the droplet, which gives rise to an interfacial Marangoni stress. The rotational component of flow in a simple shear flow, however, redistributes the surfactant, enhancing the uniformity in surface tension and hence reducing the deformation. Recently, Vlahovska *et al.* [27] have investigated the droplet deformation and bulk rheology in linear flows. They have given a small-deformation theory for the limiting case of convection-dominated surfactant transport. In a recent study, slender body theory has been used by Booty *et al.* [34] to analytically study a highly deformable bubble. Numerical simulations have also been performed to investigate large as well as transient deformations and also breakup of a surfactant-laden droplet suspended in a linear flows [17,20,22,28,29].

Some of the recent state-of-the-art problems that clearly demonstrate the efficacies of an asymptotic approach include studies on droplet migration [30], deformation [31–33], or on the bulk rheology of droplet suspensions [34–36]. However, a comprehensive analysis for the limiting case when the surfactant transport is dominated by surface diffusion is missing from the literature. This limiting case may arise in situations where the surface diffusivity of the surfactants is high. Experiments with a high value of surface diffusivity and a low imposed shear (or extensional) rate have been performed previously [37]. It can be noted here that Stone and Leal have investigated the same problem, but they have restricted their analysis up to first correction in droplet shape. Determination of higher-order solution is more of a challenge, as all the boundary conditions needs to be evaluated at the deformed boundary [38]. Here, we analytically study the effect of Marangoni stress on the dynamics of a surfactant-laden droplet in linear flows. An asymptotic study, although an approximate one, gives a sound physical insight of the overall problem and a clear understanding of the different outcomes as compared to any numerical approach. With this analysis, we can easily predict the nature of droplet deformation and subsequent effect of droplet deformation on the effective viscosity of the emulsion under different conditions of varying surfactant concentration or strength of imposed flow. The surfactants in the present problem are bulk-insoluble and get transported only along the droplet surface. As an example, we have considered two kinds of linear flows: uniaxial extensional flow and simple shear flow. For each of these linear flows, we have obtained the deformed shape of the droplet and associated modification in the bulk rheology of a dilute emulsion.

II. THEORETICAL MODEL

A. Physical system

The physical system considered in this problem consists of a neutrally buoyant droplet suspended in a linear flow. The droplet has a radius of a and is covered with bulk-insoluble surfactants, which

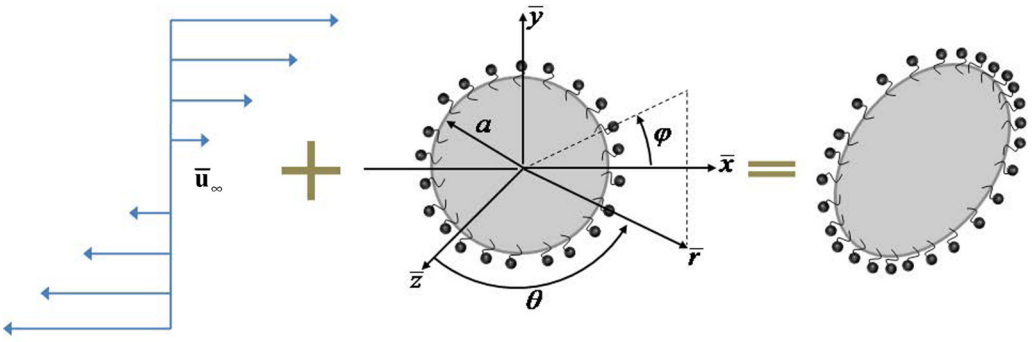

FIG. 1. Schematic of a surfactant-laden droplet of radius a suspended in a linear flow. As an example, we have shown the background flow to be a simple shear flow. Both the spherical $(\bar{r},\theta,\varphi)$ as well as the Cartesian coordinates $(\bar{x},\bar{y},\bar{z})$ are shown.

are transported along the droplet interface due to surface diffusion and convection. The viscosity of the droplet as well as the suspending phase are μ_i and μ_e, respectively. The subscript i is used to denote the droplet phase quantities, whereas the subscript e refers to the quantities related to the suspending phase. In the present study, we have considered the droplet to be suspended in a linear flow, which may be uniaxial extensional flow or simple shear flow. This imposed flow field $\bar{\mathbf{u}}_\infty$ can be represented mathematically in a general form as

$$\bar{\mathbf{u}}_\infty = (\bar{\mathbf{D}}_\infty + \bar{\mathbf{\Omega}}_\infty)\cdot\bar{\mathbf{x}}, \tag{1}$$

where $\bar{\mathbf{D}}_\infty$ is the rate of strain tensor, $\bar{\mathbf{x}}$ is the position vector, and $\bar{\mathbf{\Omega}}_\infty$ is the vorticity. For a simple shear flow we have in the above expression

$$\bar{\mathbf{D}}_\infty = \frac{\dot{\gamma}}{2}\begin{bmatrix}0 & 1 & 0\\ 1 & 0 & 0\\ 0 & 0 & 0\end{bmatrix}, \quad \bar{\mathbf{\Omega}}_\infty = \frac{\dot{\gamma}}{2}\begin{bmatrix}0 & 1 & 0\\ -1 & 0 & 0\\ 0 & 0 & 0\end{bmatrix}, \tag{2}$$

where $\dot{\gamma}$ is the shear rate. For a uniaxial extensional flow, on the other hand, we have

$$\bar{\mathbf{D}}_\infty = \frac{\dot{\gamma}}{2}\begin{bmatrix}-1 & 0 & 0\\ 0 & -1 & 0\\ 0 & 0 & 2\end{bmatrix}, \quad \bar{\mathbf{\Omega}}_\infty = 0. \tag{3}$$

A schematic of the system is given in Fig. 1, where we have only shown the case in which a surfactant-laden droplet is suspended in a simple shear flow. A spherical coordinate system $(\bar{r},\theta,\varphi)$ and a Cartesian coordinate system $(\bar{x},\bar{y},\bar{z})$ are attached to the centroid of the droplet. In the absence of any surfactant, that is for a clean droplet, the surface tension of the suspended droplet is constant and is denoted by $\bar{\sigma}_c$. On the other hand, a surfactant-laden droplet suspended in a quiescent fluid with no imposed flow has a uniform surfactant distribution $\bar{\Gamma}_{\rm eq}$ with a corresponding constant surface tension $\bar{\sigma}_{\rm eq}$. Presence of an imposed flow, however, renders the surfactant distribution nonuniform, which results in the variation of surface tension along the droplet surface. This variation in surface tension is responsible for the generation of Marangoni stress, which not only causes deformation of the droplet but also drives fluid flow. The aim of the present study is to analyze the effect of surfactants on the droplet deformation for both types of imposed flows: uniaxial extensional flow and simple shear flow. We also, in either of these cases, investigate the effect of surfactant concentration on the emulsion rheology. Toward this, we find out the effective extensional viscosity and the effective shear viscosity of a dilute emulsion comprising of deformable droplets in uniaxial extensional flow and simple shear flow, respectively.

B. Important assumptions

To analytically solve the above problem, some assumptions have to be made to simplify the governing equations as well as boundary conditions for flow field. These assumptions are as follows:

(i) The pressure, viscous and surface tension forces dominate the flow dynamics in comparison to the inertia force. In other words, the flow Reynolds number, $\mathrm{Re} = \rho\dot{\gamma}a^2/\mu_e$, is assumed to be small ($\mathrm{Re} \ll 1$). Here ρ is the density of either of the phases.

(ii) The transport of surfactants is assumed to take place only along the droplet surface, without any net flux into either of the phases. That is, the surfactant is considered to be bulk-insoluble.

(iii) The surface tension at the droplet interface is assumed to be linearly related to the local surfactant concentration.

(iv) The droplet dynamics is assumed to be unaffected by any bounding walls, if present. That is, the droplet radius is assumed to be much smaller as compared to the droplet-wall distance.

(v) The droplet is assumed to be approximately spherical, that is, only small deformations are considered. For creeping flow, the droplet deformation is governed by the magnitude of the capillary number ($\mathrm{Ca}^* = \mu_e\dot{\gamma}a/\bar{\sigma}_c$), which is the ratio of viscous force to the surface tension force acting on the droplet. In this problem we assume small deformation of the droplet only, which restricts us to small values of capillary number ($\mathrm{Ca}^* \ll 1$).

C. Governing equations and boundary conditions

We first start by stating the governing equations for flow field. The flow field, under the above assumptions, is governed by the Stokes and continuity equations, whereas the surfactant transport along the droplet surface is governed by a convection-diffusion equation [27]. The flow field is subjected to kinematic and stress balance conditions at the droplet interface, which along with the surfactant transport equation are used to solve the velocity field, the surfactant distribution, and finally the shape deformation of the droplet. We first state the characteristic scales used to nondimensionalize the set of governing equations and boundary conditions. All the dimensionless quantities and material properties in the above equations are denoted without overbar. The nondimensional scheme used is given by

$$\begin{aligned} &r = \bar{r}/a, \quad \mathbf{u} = \bar{\mathbf{u}}/\dot{\gamma}a, \quad \Gamma = \bar{\Gamma}/\bar{\Gamma}_{\mathrm{eq}}, \quad \sigma = \bar{\sigma}/\bar{\sigma}_c, \\ &p = \bar{p}/(\mu_e\dot{\gamma}), \quad \boldsymbol{\tau} = \bar{\boldsymbol{\tau}}/(\mu_e\dot{\gamma}). \end{aligned} \tag{4}$$

Different dimensionless parameters that will be useful while deriving the dimensionless form of governing equations and boundary conditions are (i) the viscosity ratio, $\lambda = \mu_i/\mu_e$, (ii) the surface Péclet number, $\mathrm{Pe}_s = \dot{\gamma}a^2/D_s$, which signifies the relative importance of convection in the transport of surfactants along the droplet surface with respect to surface diffusion, D_s being the surface diffusivity of the surfactant, (iii) the elasticity number, $\beta = \bar{\Gamma}_{\mathrm{ref}}R\bar{T}_o/\bar{\sigma}_c = -d(\bar{\sigma}/\bar{\sigma}_c)/d\bar{\Gamma}$, which indicates the sensitivity of surface tension toward local surfactant concentration, and (iv) the modified capillary number, $\mathrm{Ca} = \mathrm{Ca}^*/(1-\beta)$. The main reason for the use of the modified capillary number is that it is defined based on the equilibrium surface tension for a surfactant-laden droplet ($\bar{\sigma}_{\mathrm{eq}} = \bar{\sigma}_c(1-\beta)$) rather than the surface tension for a clean droplet ($\bar{\sigma}_c$). Such a choice adds to our convenience in further calculation [20].

Thus, using the above nondimensional scheme, the following set of nondimensional governing differential equations for flow field are obtained:

$$\begin{aligned} -\nabla p_i + \lambda\nabla^2\mathbf{u}_i = 0, \quad \nabla\cdot\mathbf{u}_i = 0, \\ -\nabla p_e + \nabla^2\mathbf{u}_e = 0, \quad \nabla\cdot\mathbf{u}_e = 0, \end{aligned} \tag{5}$$

where $\mathbf{u}_{i,e}$ is the velocity field and $p_{i,e}$ is the pressure field. The relevant boundary conditions are given by [39]

$$\text{at } r \to \infty, \quad (\mathbf{u}_e, p_e) = (\mathbf{u}_\infty, p_\infty), \quad \mathbf{u}_i \text{ is bounded at } r = 0, \quad \text{at } r = r_s, \quad \mathbf{u}_i \cdot \mathbf{n} = \mathbf{u}_e \cdot \mathbf{n} = 0,$$
$$\text{at } r = r_s, \quad \mathbf{u}_i = \mathbf{u}_e, \quad \text{at } r = r_s, \quad (\boldsymbol{\tau}_e \cdot \mathbf{n} - \boldsymbol{\tau}_i \cdot \mathbf{n}) = \frac{\beta}{(1-\beta)\mathrm{Ca}} \nabla_s \Gamma + \frac{\sigma}{\mathrm{Ca}} (\nabla \cdot \mathbf{n}). \tag{6}$$

where $\mathbf{u}_\infty$ and p_∞ are the velocity and pressure at far-field, respectively. The dimensional velocity at the far-field is provided in Eq. (1). Inside the droplet, the velocity and pressure fields $(\mathbf{u}_i, p_i)$ are bounded at the centroid of the droplet, $r = 0$. The boundary conditions at the interface of the droplet $(r = r_s)$, where r_s is the radial position of the droplet interface, consists of the kinematic boundary condition, the no-slip condition, and finally the balance between hydrodynamic and Marangoni stresses.

The radial position of the deformed droplet can be represented as $r_s = 1 + g(\theta, \varphi)$, where $g(\theta, \varphi)$ is the deviation in drop shape from sphericity. In Eq. (6) $\nabla_s = (\mathbf{I} - \mathbf{nn}) \cdot \nabla$ is the surface gradient tensor and $\mathbf{n}$ is the unit vector normal to the droplet surface and is given by

$$\mathbf{n} = \frac{\nabla F}{|\nabla F|}, \tag{7}$$

where $F = r - r_s$ is the equation for the droplet surface. $\boldsymbol{\tau}_e$ and $\boldsymbol{\tau}_i$ are the external and internal viscous/hydrodynamic stress tensors, given by [40,41]

$$\boldsymbol{\tau}_i = -p_i \mathbf{I} + \lambda [\nabla \mathbf{u}_i + (\nabla \mathbf{u}_i)^T],$$
$$\boldsymbol{\tau}_e = -p_e \mathbf{I} + [\nabla \mathbf{u}_e + (\nabla \mathbf{u}_e)^T]. \tag{8}$$

The last of the above set boundary conditions in Eq. (6) is obtained as a result of substitution of the nondimensional form of the equation of state [42], given by

$$\sigma = 1 - \beta \Gamma. \tag{9}$$

The surface tension based on the modified capillary number can be written in the following form

$$\sigma = \frac{\bar{\sigma}}{\bar{\sigma}_c (1 - \beta)}. \tag{10}$$

From the above equation it can be said that $0 < \beta < 1$. Under the assumption of bulk insolubility, the surfactant transport at steady state is governed by a convection-diffusion equation which in its dimensionless form can be written as [43]

$$\mathrm{Pe}_s \nabla_s \cdot (\mathbf{u}_s \Gamma) = \nabla_s^2 \Gamma. \tag{11}$$

The mass conservation constraint to be satisfied by the local surfactant concentration along the droplet surface can expressed in the following form:

$$\int_{\varphi=0}^{2\pi} \int_{\theta=0}^{\pi} \Gamma(\theta, \varphi) r_s^2 \sin\theta \, d\theta \, d\varphi = 4\pi. \tag{12}$$

Before attempting to solve the problem approximately, we discuss the mathematical complexities associated with the problem which restricts one to obtain an exact solution for arbitrary values of Ca and Pe_s. Exact analytical solution is not possible for any value of Ca because the droplet shape is not known *a priori*. The deformed shape of the droplet has to be obtained as a part of the solution, which can be accomplished in the regime of small deformation (i.e., $\mathrm{Ca} \ll 1$). Even when the droplet shape is nearly spherical, we cannot solve for the flow field and surfactant distribution due to the coupled nature of flow and surfactant transport. It is apparent from Eq. (11) that the surfactant transport equation is coupled to the flow field via the surface convection term on the left-hand side of the equation. Thus, exact solution cannot be obtained for any value of Pe_s. Fortunately, an asymptotic approach just serves the purpose [19,27]. It is convenient to employ a small-deformation

theory considering $\mathrm{Ca} \ll 1$. In the limit of small droplet deformation, we can progress in two different ways to study two important limiting cases: (i) diffusion-dominated surfactant transport (i.e., $\mathrm{Pe_s} \ll 1$), and (ii) convection-dominated surfactant transport (i.e., $\mathrm{Pe_s} \gg 1$). In the present study, we focus on the diffusion-dominated regime. Note that Vlahovska *et al.* [27] have employed a similar small-deformation analysis for the convection-dominated regime.

III. ASYMPTOTIC SOLUTION

In the limiting case of $\mathrm{Pe_s} \ll 1$, the surfactant transport is dominated by the surface diffusion in comparison to convection at the droplet interface. The magnitude of Pe_s is taken to be of the same order as that of capillary number (Ca), that is $\mathrm{Pe}_s \sim \mathrm{Ca}$. This can be written in the following form

$$\mathrm{Pe}_s = k\mathrm{Ca}, \tag{13}$$

where $k = a\bar{\sigma}_c(1-\beta)/\mu_e D_s$ is called the property parameter as it depends on the various material properties. Here we have assumed that k has a magnitude of $O(1)$, which is consistent with $\mathrm{Pe}_s \sim \mathrm{Ca}$. Thus, the droplet deformation is solely a function of Ca for any given values of k, β, and λ. The modified surfactant transport equation for this limiting case can be expressed as

$$k\mathrm{Ca}\nabla_s \cdot (\mathbf{u}_s\Gamma) = \nabla_s^2\Gamma. \tag{14}$$

For the other limiting case of convection-dominated surfactant transport along the droplet surface ($\mathrm{Pe_s} \to \infty$), the surfactant transport equation reduces to

$$\nabla_s \cdot (\mathbf{u}_s\Gamma) = 0. \tag{15}$$

Vlahovska *et al.* [27] have employed Eq. (15) in their analysis, which does not contain the diffusion term. Note that a slight rearrangement of Eq. (14) reduces to Eq. (15) in the limit of $k \to \infty$. Thus, the present analysis simplifies to the analysis of Vlahovska *et al.* [27] in the limit of $k \to \infty$.

In the present study, we choose the capillary number as the perturbation parameter. All the field variables can thus be expanded in a power series as follows [27]:

$$\psi = \psi^{(0)} + \psi^{(\mathrm{Ca})}\mathrm{Ca} + O(\mathrm{Ca}^2), \tag{16}$$

where ψ is any generic dependent variable. The first term in the above expansion represents the leading-order term that is the variable, ψ for no deformation. All the other terms are $O(\mathrm{Ca})$ or higher-order correction terms due to deformation of the droplet. The surfactant concentration, on the other hand, is expanded as follows [27]:

$$\Gamma = 1 + \Gamma^{(0)}\mathrm{Ca} + \Gamma^{(\mathrm{Ca})}\mathrm{Ca}^2 + O(\mathrm{Ca}^3). \tag{17}$$

Note that the surfactant concentration obtained at each order of perturbation should always satisfy the mass conservation constraint on the droplet surface as given in Eq. (12).

Toward obtaining an asymptotic solution, we express all the different quantities involved in terms of spherical harmonics. At each order of perturbation, the local surfactant concentration is expressed in the form of an infinite series in terms of spherical surface harmonics as follows:

$$\Gamma = \sum_{n=0}^{\infty}\sum_{m=0}^{n}[\Gamma_{n,m}\cos(m\varphi) + \hat{\Gamma}_{n,m}\sin(m\varphi)]P_{n,m}(\cos\theta), \tag{18}$$

where $P_{n,m}(\cos\theta)$ are the associated Legendre polynomials of order m and degree n. The unknown coefficients, $\Gamma_{n,m}$ and $\hat{\Gamma}_{n,m}$, are found out by solving the surfactant transport equation. As both the flow inside as well as outside the droplet satisfies the Stokes equations, the use of Lamb's general solution can be made to find out the velocity and pressure fields in either of the phases. The detailed expression for the Lamb's general solution is provided in the supporting material. Here we discuss the important steps towards obtaining the solution. The velocity and pressure fields can be obtained

with the help of the boundary conditions at the droplet interface namely the kinematic boundary condition, the no-slip condition and the tangential stress balance. The tangential stress boundary condition can be obtained from the stress balance condition as given in the last of the equations in Eq. (6). The tangential stress boundary condition represents the balance between the tangential component of the jump in hydrodynamic stress and the tangential component of surfactant-induced Marangoni stress. This boundary condition can be written in the following form:

$$\text{at } r = r_s, \quad (\boldsymbol{\tau}_e \cdot \mathbf{n} - \boldsymbol{\tau}_i \cdot \mathbf{n}) \cdot (\mathbf{I} - \mathbf{nn}) = \frac{\beta}{(1-\beta)\text{Ca}} (\nabla_s \Gamma) \cdot (\mathbf{I} - \mathbf{nn}), \tag{19}$$

where $\mathbf{I}$ is an identity tensor. The radial distance of the deformed surface of the drop, r_s, can be written in the following form [27]:

$$r_s = 1 + \text{Ca} g^{(\text{Ca})} + \text{Ca}^2 g^{(\text{Ca}^2)} + O(\text{Ca}^3), \tag{20}$$

where $g^{(\text{Ca})}$ and $g^{(\text{Ca}^2)}$ are $O(\text{Ca})$ and $O(\text{Ca}^2)$ correction to the spherical shape of the droplet, respectively.

We next proceed towards obtaining the solution for flow field with the help of the following steps

(i) We first substitute Eqs. (13), (16), and (17) into Eqs. (5), (6), and (11) to obtain the governing differential equations and boundary conditions for leading-order and $O(\text{Ca})$ problems.

(ii) The boundary conditions (other than the normal stress boundary condition) and the surfactant transport equation for leading-order are next solved simultaneously to calculate the flow field and surfactant concentration.

(iii) With the leading-order solution at hand, we further calculate the $O(\text{Ca})$ deformation, which can be obtained from the normal stress balance at the deformed interface of the droplet. The normal stress balance obtained from the stress balance equation given in Eq. (6) is written as

$$\text{at } r = r_s, \quad (\boldsymbol{\tau}_e \cdot \mathbf{n} - \boldsymbol{\tau}_i \cdot \mathbf{n}) \cdot \mathbf{n} = \frac{\sigma}{\text{Ca}} (\nabla \cdot \mathbf{n}). \tag{21}$$

(iv) Thus, expanding the stress tensors as shown in Eq. (16), substituting the expression of $\mathbf{n}$ from Eq. (7) and σ from Eq. (9), and applying the orthogonality condition for the associate Legendre polynomials on either sides of the normal stress balance we get the expression for $O(\text{Ca})$ correction to the droplet shape, which is given by

$$g^{(\text{Ca})} = \sum_{n=0}^{\infty} \sum_{m=0}^{n} \left[L_{n,m}^{(\text{Ca})} \cos(m\varphi) + \hat{L}_{n,m}^{(\text{Ca})} \sin(m\varphi) \right] P_{n,m}(\cos\theta), \tag{22}$$

where $L_{n,m}^{(\text{Ca})}$ and $\hat{L}_{n,m}^{(\text{Ca})}$ are constant coefficients.

(v) With the leading-order solution as well as $O(\text{Ca})$ deformation at our disposal, we proceed further towards calculating the $O(\text{Ca})$ solution for flow field and $O(\text{Ca}^2)$ correction to the droplet shape. We first start by deriving the $O(\text{Ca})$ boundary conditions and surfactant transport equation at the deformed surface of the droplet.

(vi) These equations are then solved simultaneously to obtain the $O(\text{Ca})$ flow field and surfactant concentration.

(vii) Next, we again use the orthogonality condition for associated Legendre polynomials on the either sides of the $O(\text{Ca})$ normal stress balance to calculate the $O(\text{Ca}^2)$ correction to the droplet shape. This correction in droplet shape is given by

$$g^{(\text{Ca}^2)} = \sum_{n=0}^{\infty} \sum_{m=0}^{n} \left[L_{n,m}^{(\text{Ca}^2)} \cos(m\varphi) + \hat{L}_{n,m}^{(\text{Ca}^2)} \sin(m\varphi) \right] P_{n,m}(\cos\theta). \tag{23}$$

A detailed representation of the asymptotic analysis is given in a separate supporting material, where we have mentioned the governing equations and boundary conditions for each order of perturbation. We now put forward the expressions for the surfactant concentration and the corrections

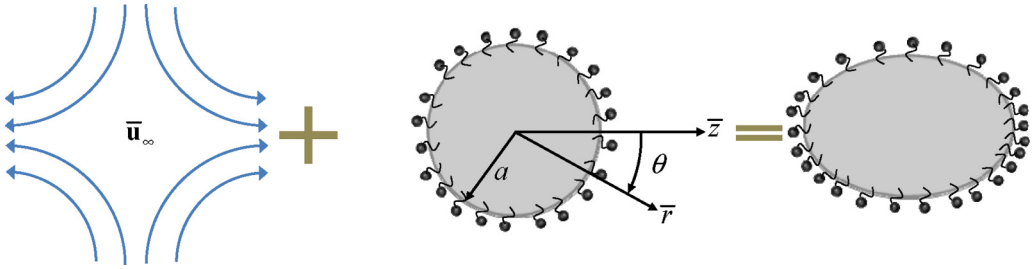

FIG. 2. Schematic of a surfactant-laden droplet suspended in a uniaxial extensional flow with $\bar{z}$ being the axis of extension. Both the imposed flow field as well as non-uniform distribution of surfactants are responsible for the deformation of the droplet.

to the droplet shape for the following two separate cases: (a) uniaxial extensional flow and (b) simple shear flow.

A. Uniaxial extensional flow field

A schematic for the case of a surfactant-laden droplet suspended in a uniaxial extensional flow field is shown in Fig. 2. The velocity as well as the pressure fields for this special case are given in Appendix A. The surfactant concentration at the droplet interface when a uniaxial extensional flow is imposed in the far-field is given by Eq. (17). The expressions for $\Gamma^{(0)}$ and $\Gamma^{(\mathrm{Ca})}$ are of the form

$$\Gamma^{(0)} = \Gamma^{(0)}_{2,0} P_{2,0} \quad \text{and} \quad \Gamma^{(\mathrm{Ca})} = \Gamma^{(\mathrm{Ca})}_{2,0} P_{2,0} + \Gamma^{(\mathrm{Ca})}_{4,0} P_{4,0}, \tag{24}$$

where the unknown coefficients are obtained as

$$\begin{aligned}
\Gamma^{(0)}_{2,0} &= \frac{5k}{2}\left(\frac{1-\beta}{5+k\beta+5\lambda-5\beta-5\lambda\beta}\right),\\
\Gamma^{(\mathrm{Ca})}_{2,0} &= -25k\frac{(g1_{2,0}\beta^3+g2_{2,0}\beta^2+g3_{2,0}\beta+g4_{2,0})}{112(\beta k-5\beta-5\beta\lambda+5+5\lambda)^3},\\
\Gamma^{(\mathrm{Ca})}_{4,0} &= -45k\frac{(g1_{4,0}\beta^3+g2_{4,0}\beta^2+g3_{4,0}\beta+g4_{4,0})}{112(\beta k-5\beta-5\beta\lambda+5+5\lambda)^2(\beta k-9\beta-9\beta\lambda+9\lambda+9)},
\end{aligned} \tag{25}$$

where $g1_{i,0} \equiv \Pi(\lambda,k) \equiv g2_{i,0} \equiv g3_{i,0} \equiv g4_{i,0}$ with $i = 2,4$. The constants present in the above equation are provided in Appendix A.

The deformed shape of the surfactant-laden droplet when it is suspended in a uniaxial extensional flow field is obtained as

$$r_s = 1 + \mathrm{Ca}\left(L^{(\mathrm{Ca})}_{2,0} P_{2,0}\right) + \mathrm{Ca}^2\left(L^{(\mathrm{Ca}^2)}_{0,0} + L^{(\mathrm{Ca}^2)}_{2,0} P_{2,0} + L^{(\mathrm{Ca}^2)}_{4,0} P_{4,0}\right), \tag{26}$$

where $L^{(\mathrm{Ca}^2)}_{0,0}$ is included in the $O(\mathrm{Ca}^2)$ correction in droplet shape to take into consideration the volume conservation constraint. The volume conservation constraint is given by

$$\int_{\varphi=0}^{2\pi}\int_{\theta=0}^{\pi}\int_{r=0}^{r_s} r^2 dr \sin\theta d\theta d\varphi = \frac{4\pi}{3}. \tag{27}$$

Thus, using the above volume conservation condition, $L^{(\mathrm{Ca}^2)}_{0,0}$ is found out to be

$$L^{(\mathrm{Ca}^2)}_{0,0} = -\tfrac{1}{5}\left(L^{(\mathrm{Ca})}_{2,0}\right)^2. \tag{28}$$

The unknown coefficients present in Eq. (26) are obtained as

$$L_{2,0}^{(\mathrm{Ca})} = \frac{5}{8}\left(\frac{16-16\beta+19\lambda+4k\beta-19\lambda\beta}{5+k\beta+5\lambda-5\beta-5\lambda\beta}\right), \tag{29}$$

$$L_{2,0}^{(\mathrm{Ca}^2)} = \frac{\left\{\begin{array}{l}\left(a_0^{(20)}\lambda^3+a_1^{(20)}\lambda^2+a_2^{(20)}\lambda+a_3^{(20)}\right)\beta^3+\left(b_0^{(20)}\lambda^3+b_1^{(20)}\lambda^2+b_2^{(20)}\lambda+b_3^{(20)}\right)\beta^2\\ +\left(c_0^{(20)}\lambda^3+c_1^{(20)}\lambda^2+c_2^{(20)}\lambda+c_3^{(20)}\right)\beta+25(19\lambda+16)(601\lambda^2+893\lambda+256)\end{array}\right\}}{448(\beta k-5\beta-5\beta\lambda+5+5\lambda)^3}, \tag{30}$$

$$L_{4,0}^{(\mathrm{Ca}^2)} = \frac{\left\{\begin{array}{l}\left(a_0^{(40)}\lambda^3+a_1^{(40)}\lambda^2+a_2^{(40)}\lambda+a_3^{(40)}\right)\beta^3+\left(b_0^{(40)}\lambda^3+b_1^{(40)}\lambda^2+b_2^{(40)}\lambda+b_3^{(40)}\right)\beta^2\\ +\left(c_0^{(40)}\lambda^3+c_1^{(40)}\lambda^2+c_2^{(40)}\lambda+c_3^{(40)}\right)\beta+15(751\lambda+656)(19\lambda+16)(\lambda+1)\end{array}\right\}}{224(\beta k-5\beta-5\beta\lambda+5+5\lambda)^2(\beta k-9\beta-9\beta\lambda+9\lambda+9)}, \tag{31}$$

where the expressions for the constants $a_0^{(20)}-a_3^{(20)}$, $b_0^{(20)}-b_3^{(20)}$, $c_0^{(20)}-c_3^{(20)}$, $a_0^{(40)}-a_3^{(40)}$, $b_0^{(40)}-b_3^{(40)}$, and $c_0^{(40)}-c_3^{(40)}$ are given in Appendix A. Although the present study is for the case of $k\sim O(1)$, we still obtain the results of Vlahovska *et al.* [27] on substitution of $k\to\infty$. The surfactant transport equation for this limiting case is provided in Eq. (15). The corresponding coefficients under this limit are provided below:

$$\lim_{k\to\infty} L_{2,0}^{(\mathrm{Ca})} = \tfrac{5}{2}, \quad \lim_{k\to\infty} L_{2,0}^{(\mathrm{Ca}^2)} = \tfrac{75}{14}, \quad \lim_{k\to\infty} L_{4,0}^{(\mathrm{Ca}^2)} = \tfrac{135}{28}. \tag{32}$$

The deformation can be conveniently quantified for the case of small deformation ($\mathrm{Ca}\ll 1$) with the help of a deformation parameter, D_{fe}, which for the case of an extensional flow field is given by

$$D_{\mathrm{fe}} = \frac{r_s(\theta=0)-r_s(\theta=\pi/2)}{r_s(\theta=0)+r_s(\theta=\pi/2)}. \tag{33}$$

The above expression can be expanded in a polynomial series which can be expressed as

$$D_{\mathrm{fe}} = \left(\tfrac{3}{4}L_{2,0}^{(\mathrm{Ca})}\right)\mathrm{Ca}+\left\{\tfrac{5}{16}L_{4,0}^{(\mathrm{Ca}^2)}+\tfrac{3}{4}L_{2,0}^{(\mathrm{Ca}^2)}-\tfrac{3}{16}\left(L_{2,0}^{(\mathrm{Ca})}\right)^2\right\}Ca^2. \tag{34}$$

B. Simple shear flow field

The schematic for the special case when the imposed flow field is a simple shear flow is shown in Fig. 1. The expressions for the velocity and pressure fields are given in Appendix B. The constant coefficients in the expression of surfactant concentration of a droplet in a simple shear flow field, as shown in Eq. (17), is given by

$$\begin{aligned}\Gamma^{(0)} &= \hat{\Gamma}_{2,2}^{(0)}\sin(2\varphi)P_{2,2},\\ \Gamma^{(\mathrm{Ca})} &= \Gamma_{2,0}^{(\mathrm{Ca})}P_{2,0}+\Gamma_{4,0}^{(\mathrm{Ca})}P_{4,0}+\Gamma_{2,2}^{(\mathrm{Ca})}\cos(2\varphi)P_{2,2}+\Gamma_{4,4}^{(\mathrm{Ca})}\cos(4\varphi)P_{4,4},\end{aligned} \tag{35}$$

where the unknown coefficients present in the above equation are given in Appendix B.

The deformed shape of a surfactant-laden droplet suspended in simple shear flow is obtained as

$$\begin{aligned}r_s = \big[1 &+ Ca\left\{\hat{L}_{2,2}^{(\mathrm{Ca})}\sin(2\varphi)P_{2,2}\right\}+Ca^2\left\{L_{0,0}^{(\mathrm{Ca}^2)}+L_{2,0}^{(\mathrm{Ca}^2)}P_{2,0}+L_{4,0}^{(\mathrm{Ca}^2)}P_{4,0}\right.\\ &\left.+L_{2,2}^{(\mathrm{Ca}^2)}\cos(2\varphi)P_{2,2}+L_{4,4}^{(\mathrm{Ca}^2)}\cos(4\varphi)P_{4,4}\right\}\big],\end{aligned} \tag{36}$$

where $L_{0,0}^{(\mathrm{Ca}^2)}$ is included to satisfy the volume conservation condition given in Eq. (27). The expression of $L_{0,0}^{(\mathrm{Ca}^2)}$ thus evaluated from the volume conservation constraint is given by

$$L_{0,0}^{(\mathrm{Ca}^2)} = -\tfrac{12}{5}\left(\hat{L}_{2,2}^{(\mathrm{Ca})}\right)^2. \tag{37}$$

All the other unknown coefficients in Eq. (36) are given in Appendix B. Even though the present study is strictly valid for $k \sim O(1)$, we obtain the results of Vlahovska *et al.* [27] for a surfactant laden droplet suspended in a simple shear flow as $k \to \infty$. The corresponding coefficients [appearing in Eq. (36)] for this limiting case are given below:

$$\lim_{k\to\infty} \hat{L}_{2,2}^{(\mathrm{Ca})} = \frac{5}{12}, \quad \lim_{k\to\infty} L_{2,0}^{(\mathrm{Ca}^2)} = -\frac{25}{14}, \quad \lim_{k\to\infty} L_{2,2}^{(\mathrm{Ca}^2)} = \frac{5}{144}\left(11\lambda + 14 + \frac{\lambda+4}{2\beta}\right),$$
$$\lim_{k\to\infty} L_{4,0}^{(\mathrm{Ca}^2)} = \frac{15}{56}, \quad \lim_{k\to\infty} L_{4,4}^{(\mathrm{Ca}^2)} = -\frac{5}{448}. \tag{38}$$

The deformation parameter, D_{fl}, for the present case can be written as

$$D_{\mathrm{fl}} = \frac{\max\{r_s(\theta=\pi/2,\varphi)\} - \min\{r_s(\theta=\pi/2,\varphi)\}}{\max\{r_s(\theta=\pi/2,\varphi)\} + \min\{r_s(\theta=\pi/2,\varphi)\}}, \tag{39}$$

where D_{fl} gives a measure of the deformation of the droplet in the plane of shear ($\theta = \pi/2$), when suspended in a simple shear flow.

The steady-state angle of inclination of the droplet in the plane of shear is given by

$$\varphi_d = \frac{\pi}{4} - \frac{L_{2,2}^{(\mathrm{Ca}^2)}}{2\hat{L}_{2,2}^{(\mathrm{Ca})}}\mathrm{Ca} + O(\mathrm{Ca}^2). \tag{40}$$

The above expression is obtained by performing a Taylor series expansion about $\varphi = \pi/4$. In the limiting case of high Péclet number ($\mathrm{Pe}_s \to \infty$), the expression for φ_d in Eq. (40) matches exactly with that obtained by Vlahovska *et al.* [27] Another alternative method to calculate the inclination angle, φ_d, for a given value of θ is to find the value of φ corresponding to the maximum value of r_s.

IV. SUSPENSION RHEOLOGY

Next, we move on to the calculation of the suspension rheology of a dilute emulsion in an imposed flow, which may be a uniaxial extensional flow or a simple shear flow. Here we focus on the dilute limit which is given by $\phi \ll 1$, where ϕ is the droplet phase volume fraction. Now, we use the leading-order and $O(\mathrm{Ca})$ flow fields to determine the $O(\phi)$ and $O(\phi\mathrm{Ca})$ corrections in suspension rheology. According to Batchelor [44], the volume averaged suspension stress for a suspension of force-free particles in linear flow is given by

$$\langle\boldsymbol{\tau}\rangle = -\langle p\rangle\mathbf{I} + 2\mathbf{D}_\infty + \frac{\phi}{V_d}\mathbf{S}, \tag{41}$$

where $\mathbf{S}$ is a stresslet, which signifies the change in total stress as a result of change in velocity and stress due to the presence of a suspended particles in the flow field. It can be expressed in the following manner [44]:

$$\mathbf{S} = \int_{\varphi=0}^{2\pi}\int_{\theta=0}^{\pi}\left[\frac{1}{2}\{(\boldsymbol{\tau}\cdot\mathbf{n})\mathbf{x} + ((\boldsymbol{\tau}\cdot\mathbf{n})\mathbf{x})^T\} - \frac{1}{3}\mathbf{I}\{(\boldsymbol{\tau}\cdot\mathbf{n})\cdot\mathbf{x}\} - \{\mathbf{un} + (\mathbf{un})^T\}\right] r_s^2 \sin\theta d\theta d\varphi. \tag{42}$$

For the case of extensional flow in the far-field, the Trouton or the effective extensional viscosity of a dilute emulsion of droplets is given by

$$\frac{\mu_{\text{ext}}}{\mu_e} = \frac{\langle\bar{\tau}_{zz}\rangle - \langle\bar{\tau}_{yy}\rangle}{\mu_e\dot{\gamma}} = \frac{\langle\bar{\tau}_{zz}\rangle - \langle\bar{\tau}_{xx}\rangle}{\mu_e\dot{\gamma}}$$
$$= 3\left[1 + \frac{5}{2}\phi\left\{\frac{(-5\lambda + k - 2)\beta + 5\lambda + 2}{(k - 5 - 5\lambda)\beta + 5 + 5\lambda}\right.\right.$$
$$\left.\left. + 15\frac{\begin{array}{c}\left(m_0^{(1)}\lambda^3 + m_1^{(1)}\lambda^2 + m_2^{(1)}\lambda + m_3^{(1)}\right)\beta^3 + \left(m_0^{(2)}\lambda^3 + m_1^{(2)}\lambda^2 + m_2^{(2)}\lambda + m_3^{(2)}\right)\beta^2 \\ +\left(m_0^{(3)}\lambda^3 + m_1^{(3)}\lambda^2 + m_2^{(3)}\lambda + m_3^{(3)}\right)\beta + (19\lambda + 16)(25\lambda^2 + 41\lambda + 4)\end{array}}{56(\beta k - 5\beta - 5\beta\lambda + 5 + 5\lambda)^3}\text{Ca}\right\}\right], \tag{43}$$

where $m_i^{(j)} \equiv \Omega(k)$ with $i = 0,1,2,3$ and $j = 1,2,3$. The different constants present in the above expression are given in Appendix C.

When a simple shear flow is imposed in the suspending fluid, the effective shear viscosity of the dilute emulsion is given by

$$\frac{\mu_{\text{eff}}}{\mu_e} = \frac{\langle\bar{\tau}_{xy}\rangle}{\mu_e\dot{\gamma}} = 1 + \frac{5}{2}\left\{\frac{(-5\lambda + k - 2)\beta + 5\lambda + 2}{(-5 - 5\lambda + k)\beta + 5 + 5\lambda}\right\}\phi + O(\text{Ca}^2). \tag{44}$$

As can be seen from the above expression, there is no $O(\text{Ca})$ contribution to the effective shear viscosity. The first and second normal stress differences (N_1 and N_2) are obtained as

$$N_1 = \frac{\langle\bar{\tau}_{xx}\rangle - \langle\bar{\tau}_{yy}\rangle}{\mu_e\dot{\gamma}}$$
$$= 5\frac{\left(n_{1,0}^{(1)}\lambda^2 + n_{1,1}^{(1)}\lambda + n_{1,2}^{(1)}2\right)\beta^2 + \left(n_{2,0}^{(1)}\lambda^2 + n_{2,1}^{(1)}\lambda + n_{2,2}^{(1)}\right)\beta + (16 + 19\lambda)^2}{8(-5\beta - 5\lambda\beta + k\beta + 5 + 5\lambda)^2}\phi\text{Ca}, \tag{45}$$

$$N_2 = \frac{\langle\bar{\tau}_{yy}\rangle - \langle\bar{\tau}_{zz}\rangle}{\mu_e\dot{\gamma}}$$
$$= -\frac{5\left\{\begin{array}{c}\left(n_{1,0}^{(2)}\lambda^3 + n_{1,1}^{(2)}\lambda^2 + n_{1,2}^{(2)}\lambda + n_{1,3}^{(2)}\right)\beta^3 + \left(n_{2,0}^{(2)}\lambda^3 + n_{2,1}^{(2)}\lambda^2 + n_{2,2}^{(2)}\lambda + n_{2,3}^{(2)}\right)\beta^2 \\ +\left(n_{3,0}^{(2)}\lambda^3 + n_{3,1}^{(2)}\lambda^2 + n_{3,1}^{(2)}\lambda + n_{3,3}^{(2)}\right)\beta + 10(19\lambda + 16)(29\lambda^2 + 61\lambda + 50)\end{array}\right\}}{112\,(k\beta - 5\lambda\beta - 5\beta + 5 + 5\lambda)^3}\phi\text{Ca}, \tag{46}$$

where $n_{i,j}^{(1)} \equiv \Xi(k) \equiv n_{i,j}^{(2)}$ with $i = j = 1,2,3$. The expressions of these constants are provided in Appendix C. We again obtain the results of Vlahovska *et al.* for bulk rheology in the limiting case of $k \to \infty$ although our theory considers a finite value of $k(\sim 1)$.

V. RESULTS AND DISCUSSIONS

A. Droplet deformation

1. Uniaxial extensional flow

We first provide a validation for our theoretical results with the numerical results obtained by Milliken *et al.* [26].The variation of deformation parameter with capillary number is first shown in

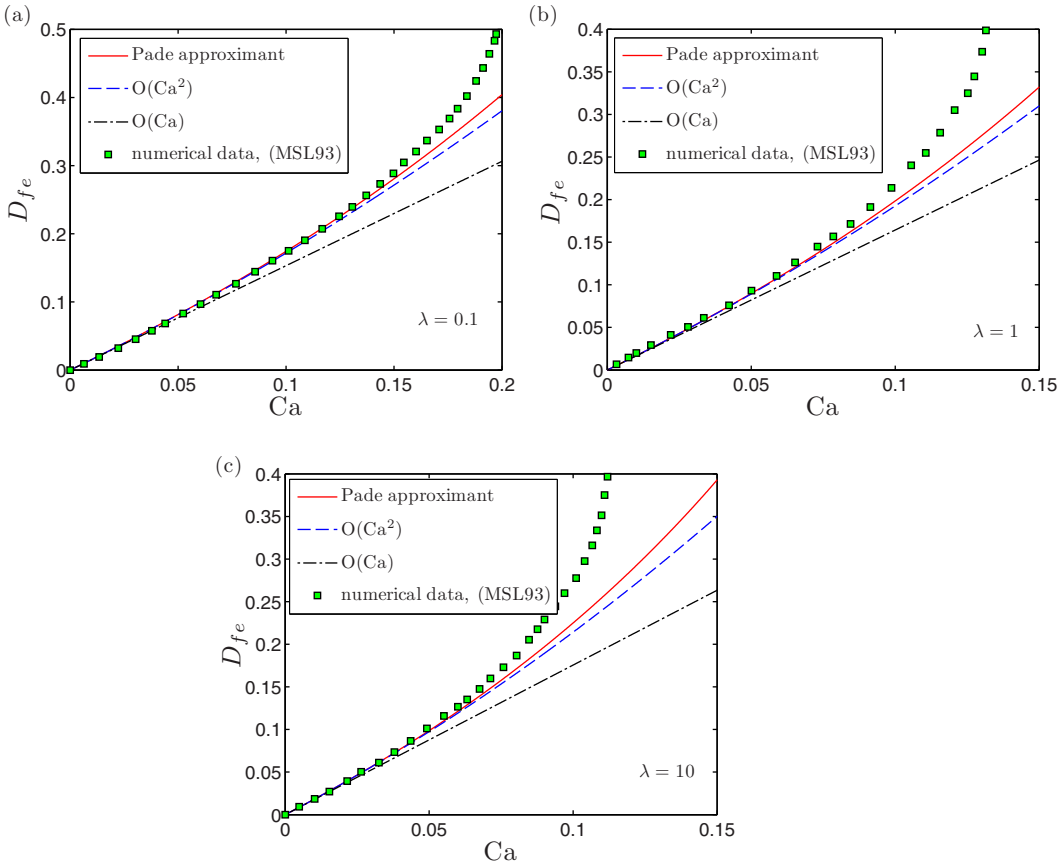

FIG. 3. Variation of deformation parameter ($D_{\rm fe}$) with Ca is shown. For (a) $\lambda = 0.1$, (b) $\lambda = 1$, and (c) $\lambda = 10$. In each of these figures numerical data from the work done by Milliken *et al.* [26] is shown along with $O(\mathrm{Ca})$ and $O(\mathrm{Ca}^2)$ solutions obtained from our theory. The value of other parameter in these plots are $\beta = 0.5$, and $k = 0.1$.

Fig. 3 for three different values of viscosity ratio (i.e., $\lambda = 0.1$, 1, 10) and for each case the results are validated with that obtained by Milliken *et al.* [26]. The other parameters used in the plot are $\beta = 0.5$ and $k = 0.1$. As can be seen from the Fig. 3, there is a good match between our $O(\mathrm{Ca}^2)$ theory and the numerical results as obtained by Milliken *et al.* [26]. In both the cases, the droplet deformation increases with Ca. The $O(\mathrm{Ca})$ theory (first developed by Stone and Leal [20]), however, deviates from the numerical results at a much earlier point. It is also seen that the match is much better for the case of a low value of $\lambda(=0.1)$ as compared to a highly viscous droplet ($\lambda = 10$). It is observed from Fig. 3 that for a fixed value of Ca, the droplet deformation reduces with decrease in λ. This result is similar to the case of a surfactant-free droplet. The effect of viscosity ratio on the deformation of a surfactant-free droplet has been investigated previously by Bentley and Leal [45].

For the purpose of an even better match between our theoretical prediction and the numerical results of Milliken *et al.* [26], we make use of Padé approximants. The Padé approximant of order $[M/N]$ for droplet deformation parameter, $D_{\rm fe}$, can be expressed as [43,46]

$$D_{p,\mathrm{fe}}[M/N] = \frac{\sum_{n=0}^{N} p_n \mathrm{Ca}^n}{1 + \sum_{n=1}^{M} q_n \mathrm{Ca}^n} \tag{47}$$

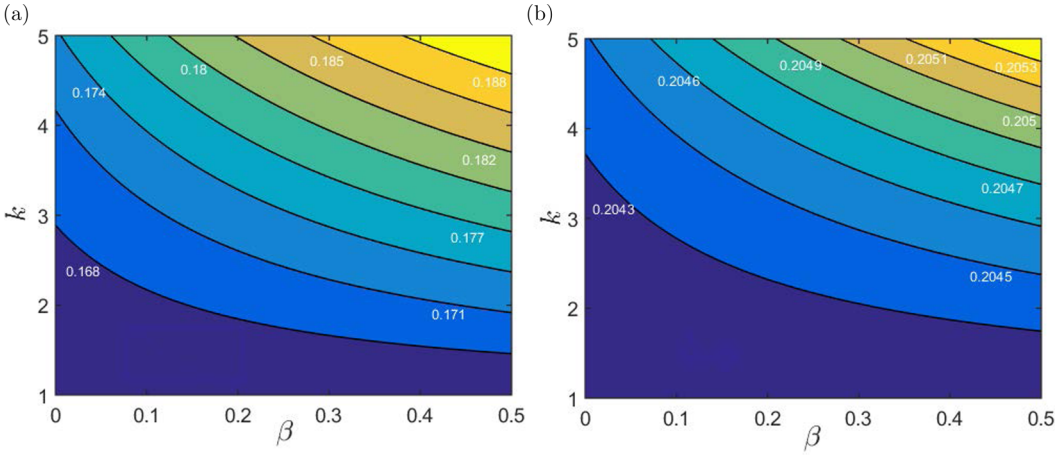

FIG. 4. Contour plot showing the variation of deformation parameter (D_{fe}) with β and k. For (a) $\lambda = 0.1$, while in (b) $\lambda = 10$. The values of the deformation parameter corresponding to different values of β and k are also provided in the plot above. The value of capillary number for the above plot is taken to be $\text{Ca} = 0.1$.

Thus, a Padé approximant consists of $M + N$ terms as the ratio of two power series in Ca of degree M and N. For the present analysis, we use a $[1/1]$ Padé approximant. We obtain the constants p_0, p_1, and q_1 by comparing the expression in Eq. (47) with the expression for the deformation parameter as given in Eq. (34) and then equating like coefficients of Ca. The $[1/1]$ Padé approximant thus obtained is provided below:

$$D_{p,\text{fe}} = \frac{9\left(L_{2,0}^{(\text{Ca})}\right)^2 Ca}{12L_{2,0}^{(\text{Ca})} - 5\text{Ca}L_{4,0}^{(\text{Ca}^2)} - 12\text{Ca}L_{2,0}^{(\text{Ca}^2)} + 3\text{Ca}\left(L_{2,0}^{(\text{Ca})}\right)^2}. \tag{48}$$

When the above expression for deformation parameter is plotted with respect to Ca, a significant improvement in the match between our theoretical results and the numerical results of Milliken *et al.* [26] is seen. The theoretical results obtained from Padé approximants, thus, deviate from the numerical results at a much later stage.

The effect of surfactants on the deformation of the droplet provides us some interesting results. A physical insight on the effect of surfactants as well as viscosity ratio on the deformation of the droplet can be obtained with the help of a contour plot as shown in Fig. 4. The parameter k, which is the property parameter, when increased, enhances the convection of surfactants along the surface of the droplet. Due to the imposed extensional flow the surfactants start accumulating at the two tips of the droplet along the z-axis. In addition to this, if k is increased, the concentration of the surfactants further increases at the tip due to increase in convection. This results in a lower surface tension at the tips as compared to the other regions on its surface. In other words, the surface tension gradient along the surface increases with increase in k and hence the surfactant-induced Marangoni stress increases, which causes a larger deformation of the droplet as compared to a clean droplet. Also, accumulation of surfactants at the end of the droplet along the axis of elongation of the droplet requires a higher curvature and hence results in an increased deformation. It is confirmed from Fig. 4 that for a particular value of β, increase in k increases the deformation of the droplet. For a droplet having fixed concentration of surfactants along its surface (that is $\beta = 0$), the average surfactant concentration decreases upon deformation. Thus, the surface tension increases and any further deformation of the droplet reduces in comparison to a droplet having uniform surfactant distribution.

If λ is increased, or if the droplet is more viscous as compared to the suspending flow, then any change in the surface tension on the surface of the droplet (and hence the Marangoni stress) does not affect its deformation to that extent as it would had been for a low viscosity droplet. In other

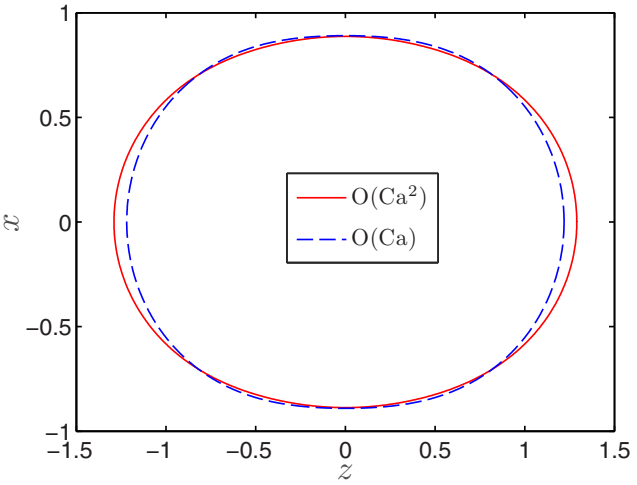

FIG. 5. Deformed shape of the droplet at different orders of perturbation. The different parameters involved in this plot are $\beta = 0.5$, $k = 0.1$, $\lambda = 1$, and $\mathrm{Ca} = 0.1$.

words, the reduction in surface velocity of the droplet, due to increase in Marangoni stress, does not contribute much to the deformation characteristics for a high viscous droplet. This is because the surface velocity is already significantly reduced due to the high viscosity of the droplet and any further reduction in the same due to variation in surfactant concentration is just incremental. This can as well be observed by comparing Figs. 4(a) and 4(b). The change in deformation parameter (D_{fe}) of a droplet with $\lambda = 10$ due to change in β or k is found to be much less in comparison to that of a droplet with $\lambda = 0.1$. It can also be said that for a high value of k (e.g., $k = 5$), the Marangoni stress is high enough to affect the deformation of the droplet and any change in λ (say from $\lambda = 0.1$ to $\lambda = 1$) has minimal effect on the same. For smaller values of k, the Marangoni stress developed is low and hence any change in λ has significant effect on the deformation of the droplet. At the same time, from Fig. 4 we can also say that an increase in the viscosity ratio (from $\lambda = 0.1$ to $\lambda = 10$) reduces the effect of surfactants on the deformation of the droplet. For $\lambda = 0.1$, the deformation parameter varies from a minimum of 0.168 to a maximum of 0.188, whereas for $\lambda = 10$, the change in D_{fe} is way too small, that is from 0.2043 to 0.2053.

The deformed shape of the droplet, subjected to a uniaxial extensional flow is shown in Fig. 5 for different orders of perturbation, $O(\mathrm{Ca})$ and $O(\mathrm{Ca}^2)$. It is seen that due to the presence of extensional bulk flow the droplet takes the shape of an ellipsoid with its major axis aligned along the extensional axis. Higher-order correction shows that the droplet becomes more ellipsoidal. Thus, the higher-order correction has a destabilizing effect, which physically signifies the fact that with increase in Ca, the droplet will eventually breakup into fragments.

2. Simple shear flow

We first validate our result with existing experimental results of Feigl *et al.* [37]. Toward this, we first plot the variation of the parameters L, B, and W with Ca. These parameters have been previously used by Feigl *et al.* [37] to define different experimentally observed droplet dimensions. L denotes the dimensionless major axis of the deformed droplet, which increases as the surface tension force reduces in comparison to the viscous forces acting on the droplet (or as Ca increases). B indicates the minor axis of the droplet and it reduces with increase in Ca. Finally, W is the length along the vorticity axis which too reduces with increase in Ca. These parameters thus give a measure of the

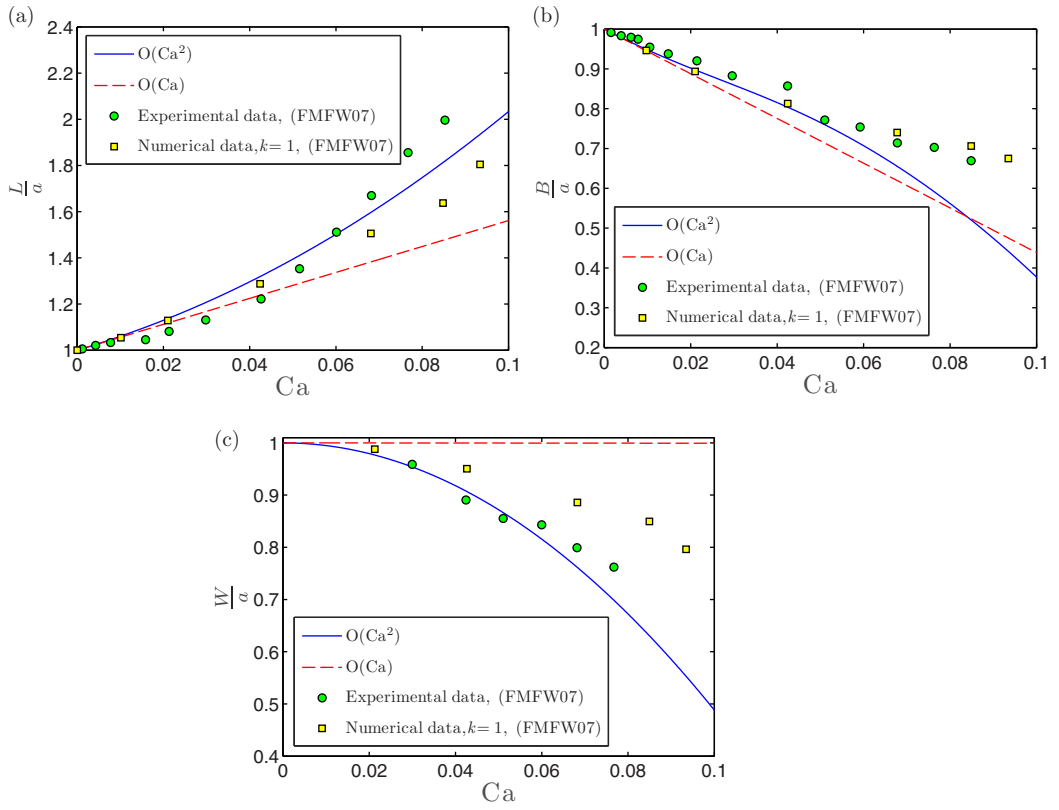

FIG. 6. Variation of $O(\mathrm{Ca})$ and $O(\mathrm{Ca}^2)$ solution for (a) L, (b) B, and (c) W with Ca. The circular and the square points indicate the experimental and numerical data points, respectively, as obtained from Fig. 4 of Feigl *et al.* [37]. The values of the other parameters are $\beta = 0.8$, $\lambda = 0.335$, and $k = 1$.

deformation of the droplet and can be expressed as

$$\begin{aligned} L &= \max_{\varphi}\{r_s(\theta = \pi/2, \varphi \in [0,\pi])\}, \\ B &= \min_{\varphi}\{r_s(\theta = \pi/2, \varphi \in [0,\pi])\}, \\ W &= \min_{\theta}\{r_s(\varphi = \pi/2, \theta \in [0,\pi/2])\}. \end{aligned} \tag{49}$$

In Fig. 6 we see that for all the three parameters (L, B, W), there is a good match between the experimental results of Feigl *et al.* [37] and our $O(\mathrm{Ca}^2)$ solution. The $O(\mathrm{Ca})$ solution, however, largely deviates from the experimental result in comparison to the higher-order solution. Due to the presence of bulk shear flow, the surfactants accumulate on either of the tips of the major axis, while there is a dearth of the same at the end of both the minor as well as the vorticity axis. Because of this nonuniform distribution of surfactants along the droplet surface, a gradient in surface tension is generated which results in Marangoni stress. This results in the deformation of the droplet.

We also compare our asymptotic results with the numerical results obtained by Feigl *et al.* [37]. In Fig. 7 we have shown the variation of L, B, and W for two different values of $k(= 0,5)$. As can be seen that for the case of $k = 5$, the match between our theoretical results and their numerical results is pretty good. For the case of an imposed simple shear flow, we do not indulge in the use of Padé approximants as there is not any significant improvement in the accuracy of the results.

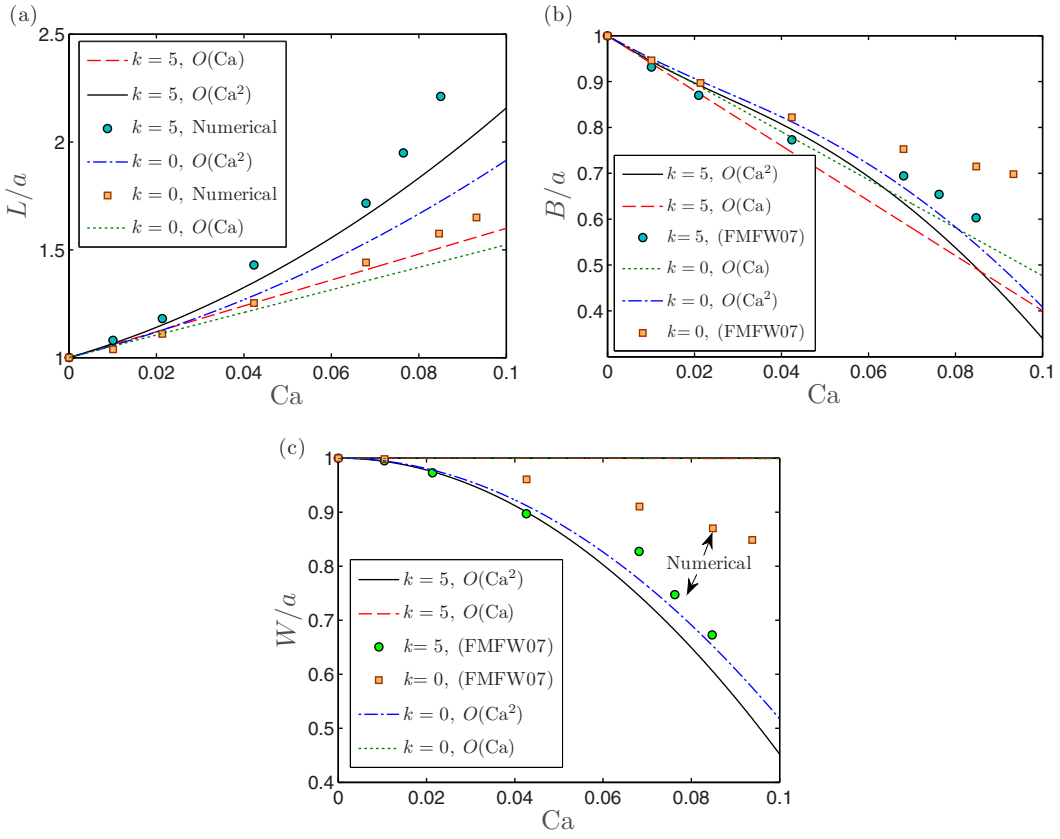

FIG. 7. Variation of $O(\mathrm{Ca})$ and $O(\mathrm{Ca}^2)$ solution for (a) L, (b) B, and (c) W with Ca. The circular and the square points indicate the experimental and numerical data points, respectively, as obtained from Fig. 4 of Feigl *et al.* [37]. The values of the other parameters are $\beta = 0.8$, $\lambda = 0.335$. Each of the above plots are drawn for $k = 0, 5$.

We next explore the effect of surfactant distribution as well as the viscosity ratio on the deformation of the droplet. Towards investigating the effect of surfactant distribution on the deformation of the droplet, we show two contour plots in Fig. 8. Figure 8(a) considers the case of a low viscous droplet with $\lambda = 0.1$, and Fig. 8(b) considers the case of a highly viscous droplet with $\lambda = 10$. It can be seen from the contour plot in Fig. 8 that increase in both β and k increases the deformation of the droplet. Increase in k increases the nonuniformity in surfactant distribution due to enhanced surfactant convection. Hence, the surface tension gradient along the droplet surface increases which further results in a higher Marangoni stress. This Marangoni stress developed due to nonuniform surfactant distribution is responsible for the droplet deformation. For low viscous droplets ($\lambda = 0.1$), the Marangoni stress plays an important role in the deformation of the droplet. For high viscous droplets ($\lambda = 10$), although the deformation of the droplet for same values of β and k is larger, the effect of Marangoni stress on droplet deformation is minimal. This can be observed by comparison of Figs. 8(a) and 8(b). It is thus seen that increase in droplet deformation due to increase in either β or k is larger for $\lambda = 0.1$ as compared to the case when $\lambda = 10$. Thus, it can be said that change in surfactant distribution along the surface of the droplet results in a significant change in deformation for a bubble ($\lambda \to 0$), where no deformation takes place for a particle ($\lambda \to \infty$).

The angle of inclination can be also theoretically predicted. In the plane of shear ($\theta = \pi/2$), the expression for angle of inclination as given in Eq. (40), when plotted against Ca, matches pretty well

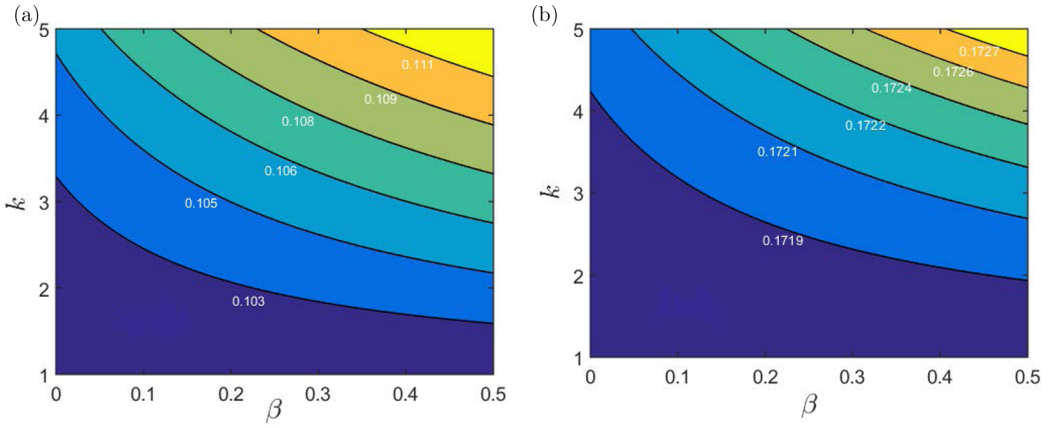

FIG. 8. Contour plot showing the variation of deformation parameter (D_{fl}) with β and k. For (a) $\lambda = 0.1$, while in (b) $\lambda = 10$. The values of the deformation parameter corresponding to different values of β and k are labeled in the plot above. The value of capillary number for the above plot is taken to be $\text{Ca} = 0.1$.

with the numerical result obtained by Li and Pozrikidis [28]. This is shown in Fig. 9(a). The effect of droplet viscosity or the viscosity ratio on the inclination angle of the droplet can be explained from Fig. 10. It is seen that higher the viscosity ratio, lower is the inclination angle for a given value of capillary number. That is, a droplet with a higher viscosity aligns itself more towards the direction of imposed flow in comparison to a low viscous droplet. It is also seen that surfactant distribution along the droplet surface has no effect on the orientation or the inclination angle of the droplet. Figure 10 is drawn for a fixed value of the polar angle, $\theta = \pi/2$. For higher Ca, change in λ has a greater effect on the orientation of the droplet suspended in a simple shear flow.

The shape of a surfactant-laden droplet suspended in a simple shear flow is shown for different orders of perturbation in Fig. 11. This figure clearly shows the orientation of the droplet as well. The

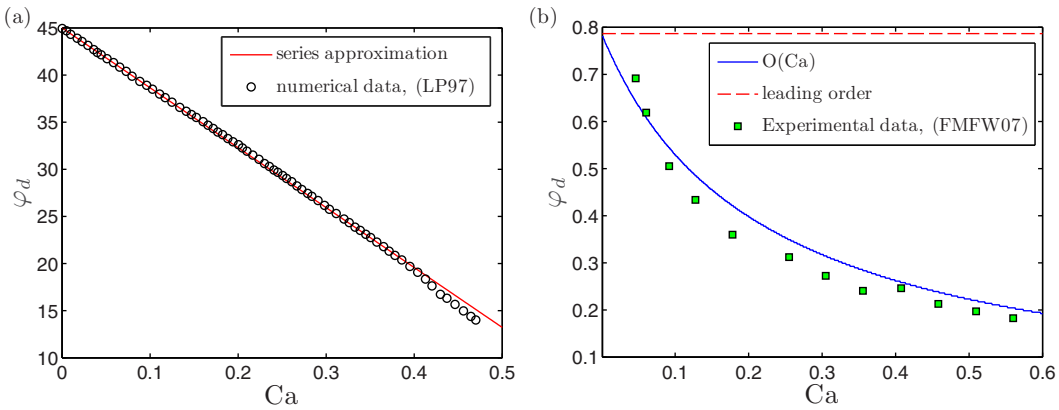

FIG. 9. Variation of inclination angle with Ca. (a) A series approximation for the inclination angle is found out [Eq. (40)] and plotted against Ca. The different parameters involved are $k = 10$, $\lambda = 1$, and $\beta = 0.1$. The marker points indicate numerical data taken from the work of Li and Pozrikidis [28]. (b) A more accurate approach is used to calculate the angle of inclination directly from the solution for the deformed droplet shape. The "green" square points denote the experimental data points from the work done by Feigl *et al.* [37]. The other parameters are $\lambda = 6.338$, $\beta = 0.5$, and $k = 5$.

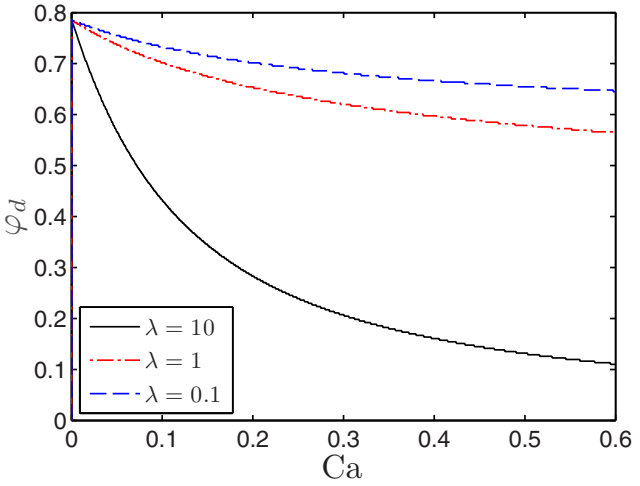

FIG. 10. Variation of the inclination angle of the droplet with Ca for different values of λ(=0.1, 1, 10). The other parameters values are $\beta = 0.5$, $k = 5$, $\lambda = 1$, and $\theta = \pi/2$.

droplet is found to elongate and take the shape of an ellipsoid with the major axis oriented along the extensional axis. The surfactants thus accumulate at the either ends of the major axis and affect the droplet deformation.

B. Suspension rheology

1. Uniaxial extensional flow

In Fig. 12 we show the variation of normalized Trouton viscosity or the effective extensional viscosity with the bulk viscosity ratio, λ. The effective extensional viscosity is normalized with respect to the volume fraction, ϕ. For the limiting case of a clean droplet $k = 0$, our theoretical result

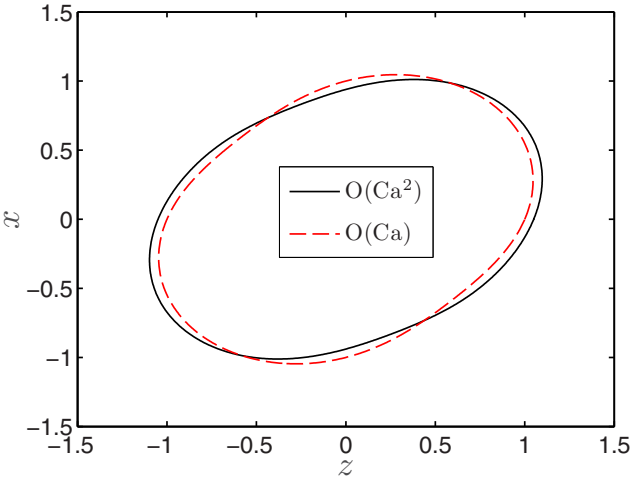

FIG. 11. Shape of the surfactant laden-droplet when suspended in a simple shear flow. Both the shapes due to $O(\mathrm{Ca})$ as well as $O(\mathrm{Ca}^2)$ corrections are shown. The different parameters used for this plot are $\beta = 0.1$, $k = 5$, $\lambda = 1$, and $\mathrm{Ca} = 0.15$.

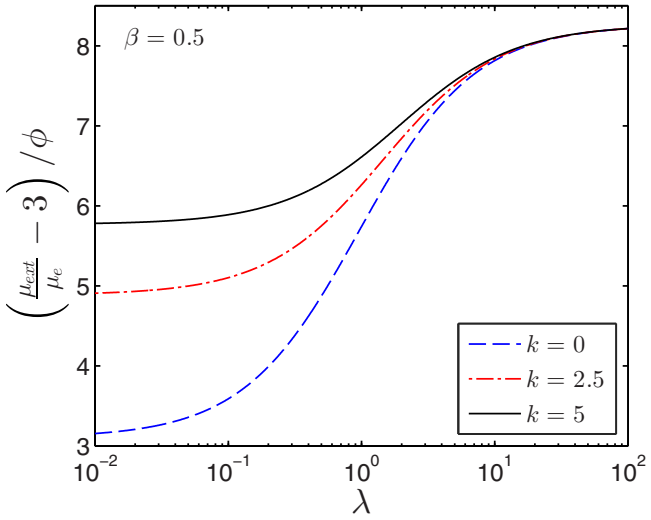

FIG. 12. Variation of normalized effective extensional viscosity with λ for different values of $k(=0, 2.5, 5)$. Variation of the normalized effective extensional viscosity with λ for a clean droplet ($k = 0$) has been shown by Ramachandran and Leal. The value of the capillary number is taken as $\mathrm{Ca} = 0.1$ and $\beta = 0.5$.

matches exactly with that obtained by Ramachandran and Leal [51] (they have considered the effect of slip in their analysis, however, we have taken the slip factor to be zero for comparison purpose). For the case of clean droplets ($k = 0$), the presence of the droplets in the suspending fluid tends to retard the imposed flow. This results in a viscosity of the emulsion which is larger than the viscosity of the bulk fluid. As the viscosity of the surfactant-free droplet increases (or as λ increases), the resistance provided by the suspended droplet increases and hence the effective extensional viscosity (μ_{ext}) increases too (see Fig. 12). In the limiting case of particle ($\lambda \to \infty$), the effective extensional viscosity is the highest. Presence of surfactants on the surface of the droplets further modifies the effective extensional viscosity. Nonuniform distribution of the surfactants induced by the bulk flow, generates a Marangoni stress due to variation of surface tension about the droplet surface. This Marangoni stress, which acts against the direction of bulk flow deforms the droplet and further increases the effective extensional viscosity of the droplet. Increase in k increases the convective transport of surfactants along the droplet surface and hence increases the non-uniformity in surfactant distribution, which in turn increases the Marangoni stress. As a result, μ_{ext} increases with increase in k. This can clearly be seen from Fig. 12. Another important observation from the same figure is that the increase in μ_{ext} with increase in k is the largest for the case of low viscous droplets. That is, the surfactant concentration on droplet surface has almost negligible effect on the effective extensional viscosity for a highly viscous droplet, as the effect of Marangoni stress is minimal. It can also be shown that the parameter β has a similar effect on the bulk rheology. The elasticity parameter, β, increases the sensitivity of surface tension towards the surfactant distribution and hence for a constant k, increase in β increases the Marangoni stress, which in turn increases the effective extensional viscosity. That is, the effect of k on bulk rheology is enhanced with increase in β.

We also show a comparison between the leading order and $O(\mathrm{Ca})$ solution for effective viscosity in Fig. 13. Shape deformation further increases the effective viscosity as evident from Fig. 13. It can be seen that the effect of shape deformation on the magnitude of normalized effective viscosity is relatively less for a low viscous droplet as compared to a highly viscous droplet. For a highly viscous droplet, the $O(\mathrm{Ca})$ correction to the droplet shape results in a higher effective viscosity in comparison to that for a spherical droplet.

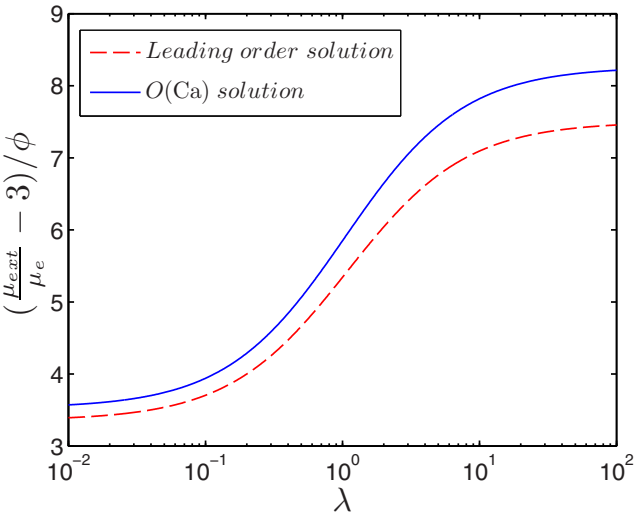

FIG. 13. Variation of normalized effective extensional viscosity with λ at different orders of perturbation. The value of other important parameters are $\beta = 0.3$, $k = 1$, and $\mathrm{Ca} = 0.1$.

2. *Simple shear flow*

The nature of variation of the effective shear viscosity (μ_{eff}) is the same as was observed for the case of effective extensional viscosity, that is, effective shear viscosity increases with increase in nonuniformity of surfactant distribution along the droplet surface. Hence, no further attempt has been made to display the variation of effective viscosity with λ for the case of an imposed simple shear flow. Note that shape deformation does not affect the effective shear viscosity. However, shape deformation leads to generation of first and second normal stress differences N_1 and N_2 in the emulsion [48]. Thus, the emulsion exhibits non-Newtonian behavior. The variation of the first and second normal stress differences, N_1 and N_2, with Ca is shown in Fig. 14. For both the cases, there is a good match between our theoretical prediction and the numerical results of Li and Pozrikidis [28]. Both the magnitude of N_1 and N_2 increase with increase in Ca. Under the assumption of negligible inertia, N_1 is positive and N_2 is negative for a dilute emulsion of droplets. This can be seen from

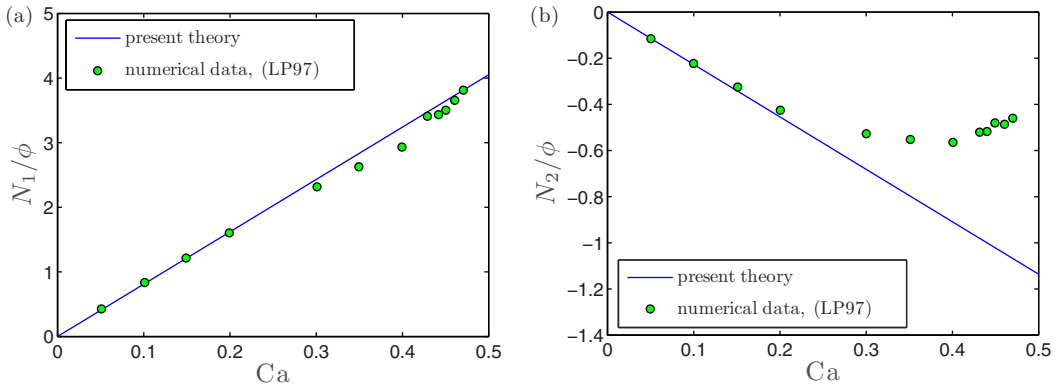

FIG. 14. (a) Variation of first normal stress difference (N_1) with Ca. (b) Variation of the second normal stress difference (N_2) with Ca. The circular points in the plot indicate the numerical result as obtained by Li and Pozrikidis [28]. The different parameters involved in either of the plots are $\beta = 0.1$, $k = 10$, and $\lambda = 1$.

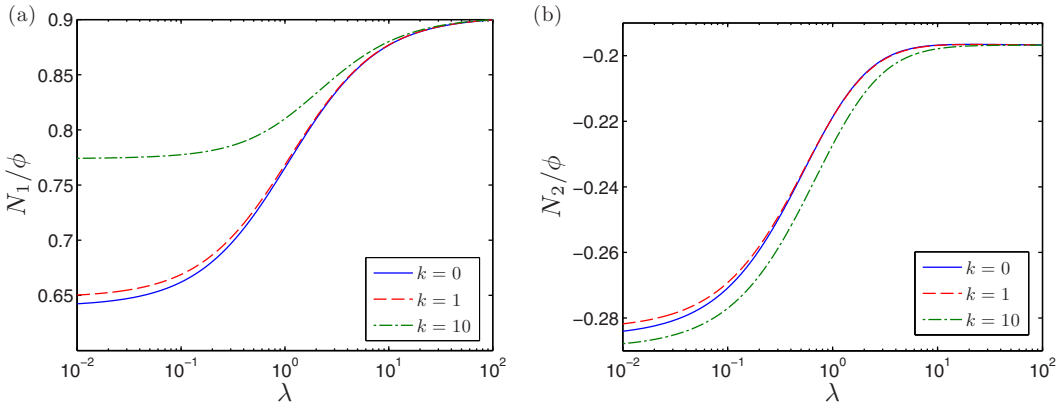

FIG. 15. (a) Variation of normalized first normal stress difference (N_1/ϕ) with λ. (b) Variation of the normalized second normal stress difference (N_2/ϕ) with λ. Each of the plots are drawn for different values of k(=0, 1, 10). The different parameters involved in either of the plots are $\beta = 0.1$ and $\mathrm{Ca} = 0.1$.

Fig. 14 as well as in Fig. 15. The sign of these normal stress differences is related to the deformation of a droplet suspended in a simple shear flow. As seen from Fig 11, at $O(\mathrm{Ca})$ the initially spherical droplet is stretched into an ellipsoidal shape with the major axis aligned along the extensional axis of the simple shear.

Finally we show the variation of N_1 and N_2 with λ for different values of k(=0, 2.5, 5) in Fig. 15. It can be seen from Fig. 15 that both the normal stresses increase with an increase in λ. There is also an increase in N_1 due to an increase in k. This increase is the largest for the case of a low viscous droplet as compared to a highly viscous droplet. At $O(\mathrm{Ca}^2)$, the shape of the droplet is unaffected by rotation and is directly proportional to the rate of strain tensor. However, the vorticity present in the simple shear bulk flow tends to rotate the ellipsoidal droplet in the flow direction. The tensile component of surface tension forces that act in this direction, thus results in a positive N_1 at $O(\mathrm{Ca})$, whereas the extra compressive stress acting on the droplet in the gradient direction causes a negative N_2 for the same order.

To investigate the effect of surfactant concentration on N_1 and N_2, we have shown the variation of the normalized first and second normal stress difference (N_1/ϕ , N_2/ϕ) with the viscosity ratio, λ for different values of k. It can be seen from Fig. 15(a) that N_1 increases as the droplet phase is made more viscous or in other words, as λ is increased. For the case of a surfactant-laden droplet the surface tension along the droplet interface varies due to the non-uniform distribution of surfactants. Thus, with an increase in k, the gradient in surface tension along the droplet surface increases. This results in an increase in the tensile component of the surface tension force along the flow direction thus elongating the droplet along the extensional axis. This in turn results in an increase in the magnitude N_1 which can be seen from Fig. 15(a). The effect of surfactant distribution on N_1 is seen to be higher for a low viscous droplet as compared to a highly viscous droplet. Now looking into Fig. 15(b), we can find that the nature of variation of N_2 is just the opposite as compared to N_1. As λ increases, the magnitude of N_2 decreases. For a low viscous droplet, if compare between a clean droplet and surfactant laden droplet, we can say that for the later the Marangoni stress generated due to non-uniform distribution of surfactants results in a compression along the gradient direction. This results in a increase of N_2 for a surfactant-laden droplet. It can be also seen from the Fig. 15(b) that an increase in the parameter k increases the convection driven surfactant transport and hence increases the magnitude of N_2. Comparison of the above plots for $k = 0$ (clean droplet) [47,48], $k = 1, k = 10$ (low surface diffusion) [27] shows that the surface diffusion plays an important role in determining the normal stress differences. That is, as the surface diffusion of surfactants reduces,

the magnitude of the normal stress differences ($|N_1|$, $|N_2|$) increases. Just like in the case of N_1, variation in N_2 due to presence of surfactants is found to be significant for a low viscous droplet as compared to a highly viscous droplet.

VI. CONCLUSIONS

In the present study, we have investigated the effect of surfactant distribution on droplet deformation as well as on the bulk rheology of a dilute emulsion of droplets. An asymptotic approach is used to analyze the problem for the limiting case when the surfactant transport along the droplet surface is dominated by the surface diffusion rather than surface convection. A regular perturbation methodology was used, with Ca as the perturbation parameter to solve the flow field in the small deformation limit. This approach has its own limitations for example, a study based on large deformations of the droplet or any arbitrary Péclet is not feasible. None the less, within the limiting regime, a perturbation analysis gives us remarkably good match with experiments and numerical simulations, which makes it an important candidate in this field and outweighs any numerical methods that brings in unnecessarily high computational costs. Based on these results a fair prediction can be made on the fate of droplet dynamics outside the limiting regime. The results thus obtained revealed various interesting outcomes, some of which are stated below:

(i) For a droplet suspended in a linear flow (uniaxial extensional or simple shear flow), increase in k or β, enhances the deformation of the droplet. This effect of surfactant concentration on the droplet deformation reduces as the droplet becomes more viscous or as λ increases.

(ii) For the case when the droplet is suspended in a simple shear flow, the inclination angle remains unaffected by any variation in the surfactant concentration along the droplet surface. However, if the viscosity of the droplet with respect to the suspending fluid is increased gradually, the droplet starts aligning itself toward the direction of flow.

(iii) Considering a dilute emulsion of droplets suspended in a linear flow field, the effective shear viscosity (effective extensional viscosity for extensional flow) of the emulsion is significantly affected by both the viscosity ratio as well as the surfactant concentration along the droplet surface. That is, increase in k, β, or λ increases the effective shear viscosity of the emulsion, although the effect of the parameter k is more significant for low value of λ.

(iv) For the case of dilute emulsion of droplets suspended in a simple shear flow, normal stress differences (N_1, N_2) are present. The first normal stress difference (N_1) is found to increase with increase in k, whereas the same also is found to increase for a higher value of λ provided k is a constant. The second normal stress difference (N_2), on the other hand, seems to be unaffected by any change in the surfactant concentration, although it reduces with increase in λ.

See the Supplemental Material for the details of the boundary conditions, governing equations, and the asymptotic analysis [49].

APPENDIX A: DIFFERENT CONSTANTS PRESENT IN THE EXPRESSIONS OF SURFACTANT CONCENTRATION AND DROPLET DEFORMATION WHEN THE BULK FLOW IS A UNIAXIAL EXTENSIONAL FLOW

The constant coefficients present in the expression for surfactant concentration as shown in Eqs. (24) and (25) are given below:

$$
\begin{aligned}
g1_{2,0} &= \{76\lambda^2 + (368 - 15k)\lambda + 256 - 60\,k + 4k^2\} \\
g2_{2,0} &= \{-228\lambda^2 + (-1104 + 10k)\lambda + -768 + 100k - 4k^2\} \\
g3_{2,0} &= \{228\lambda^2 + (1104 + 25k)\lambda - 20k + 768\} \\
g4_{2,0} &= -76\lambda^2 - (20k + 368)\lambda - 256 - 20k
\end{aligned}
\tag{A1}
$$

and

$$g1_{4,0} = \{608\lambda^2 + (1120 - 187k)\lambda + 512 - 172k + 20k^2\},$$
$$g2_{4,0} = \{-1824\lambda^2 + (-3360 + 338k)\lambda - 1536 + 308k - 20k^2\},$$
$$g3_{4,0} = \{1824\lambda^2 + (3360 - 115k)\lambda - 100k + 1536\},$$
$$g4_{4,0} = -4\,(\lambda + 1)(152\lambda + 128 + 9k). \tag{A2}$$

The expression of the constants present in Eqs. (29)–(31) for $O(\mathrm{Ca}^2)$ deformation is given by

$$a_0^{(20)} = -285475, \quad a_1^{(20)} = (174100k - 664575),$$
$$a_2^{(20)} = (270800k - 478800 - 35300k^2), \quad a_3^{(20)} = 97600\,k - 102400 + 2400\,k^3 - 27200k^2,$$
$$b_0^{(20)} = 856425, \quad b_1^{(20)} = (-348200k + 1993725),$$
$$b_2^{(20)} = (-541600k + 35200k^2 + 1436400), \quad b_3^{(20)} = 307200 + 26800k^2 - 195200k,$$
$$c_0^{(20)} = -856425, \quad c_1^{(20)} = (174100k - 1993725),$$
$$c_2^{(20)} = (-1436400 + 100k^2 + 270800k), \quad c_3^{(20)} = -307200 + 97600k + 400k^2, \tag{A3}$$

and

$$a_0^{(40)} = -214035, \quad a_1^{(40)} = (-581235 + 114600k),$$
$$a_2^{(40)} = (-19710k^2 + 209100k - 524640), \quad a_3^{(40)} = -157440 - 18120k^2 + 95040k + 1080k^3,$$
$$b_0^{(40)} = 642105, \quad b_1^{(40)} = (-229200k + 1743705),$$
$$b_2^{(40)} = (19650k^2 - 418200k + 1573920), \quad b_3^{(40)} = -190080k + 18000k^2 + 472320,$$
$$c_0^{(40)} = -642105, \quad c_1^{(40)} = (-1743705 + 114600k),$$
$$c_2^{(40)} = (209100k - 1573920 + 60k^2), \quad c_3^{(40)} = -472320 + 95040k + 120k^2. \tag{A4}$$

The expression of the velocity field both outside and inside the droplet is given below:

$$\mathbf{u}_{i,0} = \frac{15}{4}\left\{\frac{r(1-\beta)(1-r^2)}{5 + kbt + 5\lambda - 5bt - 5\lambda bt}\right\}(1 - 3\cos^2\theta)\mathbf{e}_r + \frac{15}{8}\left\{\frac{r(1-\beta)(3-5r^2)}{5 + k\beta + 5\lambda - 5\beta - 5\lambda\beta}\right\}\sin(2\theta)\mathbf{e}_\theta,$$
$$\mathbf{u}_{e,0} = \left[\frac{5}{4}\frac{\left\{\left((-5\lambda + k - 2)r^2 + 3\lambda - \frac{3}{5}k\right)bt + (5\lambda + 2)r^2 - 3\lambda\right\}}{r^4\{(k - 5 - 5\lambda)bt + 5 + 5\lambda\}}(1 - 3\cos^2\theta) + \frac{3}{2}r\cos^2\theta - \frac{1}{2}r\right]\mathbf{e}_r + \frac{3}{4}\left[\frac{\{(-5\lambda + k)bt + 5\lambda\}}{r^4\{(k - 5 - 5\lambda)bt + 5 + 5\lambda\}} - r\right]\sin(2\theta)\mathbf{e}_\theta. \tag{A5}$$

The pressure field for either of the phases are written below:

$$p_{i,0} = -\left\{\frac{105\lambda(1-\beta)r^2}{(4k - 20 - 20\lambda)bt + 20 + 20\lambda}\right\}(1 - 3\cos^2\theta),$$
$$p_{e,0} = \frac{5}{2r^3}\left\{\frac{(-5\lambda + k - 2)bt + 5\lambda + 2}{(k - 5 - 5\lambda)bt + 5 + 5\lambda}\right\}(1 - 3\cos^2\theta). \tag{A6}$$

APPENDIX B: CONSTANTS PRESENT IN THE EXPRESSIONS OF SURFACTANT CONCENTRATION AND DROPLET DEFORMATION WHEN THE BULK FLOW IS A SIMPLE SHEAR FLOW

The expression of the constant coefficients present in Eq. (35), in the expression for surfactant concentration are written below:

$$\hat{\Gamma}^{(0)}_{2,2} = \frac{5k}{12}\left\{\frac{1-\beta}{-5\beta-5\lambda\beta+5\lambda+5+k\beta}\right\},$$

$$\Gamma^{(Ca)}_{2,0} = -25k\frac{\{h1_{2,0}\beta^3+h2_{2,0}\beta^2+h3_{2,0}\beta+h4_{2,0}\}}{336(-5\beta-5\beta\lambda+\beta k+5+5\lambda)^3},$$

$$\Gamma^{(Ca)}_{4,0} = -45k\frac{\{h1_{4,0}\beta^3+h2_{4,0}\beta^2+h3_{4,0}\beta+h4_{4,0}\}}{224(\beta k-9\beta-9\beta\lambda+9\lambda+9)(-5\beta-5\beta\lambda+\beta k+5+5\lambda)^2}, \tag{B1}$$

$$\Gamma^{(Ca)}_{2,2} = 5k\frac{\{h1_{2,2}\beta^2+h2_{2,2}\beta+h3_{2,2}\}}{288(-5\beta-5\beta\lambda+\beta k+5+5\lambda)^2},$$

$$\Gamma^{(Ca)}_{4,4} = 5k\frac{\{h1_{4,4}\beta^3+h2_{4,4}\beta^2+h3_{4,4}\beta+h4_{4,4}\}}{5376(\beta k-9\beta-9\beta\lambda+9\lambda+9)(-5\beta-5\beta\lambda+\beta k+5+5\lambda)^2},$$

where

$$h1_{2,0} = \{76\lambda^2+(368-15k)\lambda+256-60\,k+4\,k^2\}$$

$$h2_{2,0} = \{-228\lambda^2+(-1104+10k)\lambda-768+100k-4k^2\}$$

$$h3_{2,0} = \{228\lambda^2+(1104+25k)\lambda-20\,k+768\}$$

$$h4_{2,0} = \{-76\lambda^2+(-20k-368)\lambda-20\,k-256\} \tag{B2}$$

$$h1_{4,0} = \{608\lambda^2+(1120-187k)\lambda+512-172k+20k^2\}$$

$$h2_{4,0} = \{-1824\lambda^2+(-3360+338k)\lambda-1536+308k-20k^2\}$$

$$h3_{4,0} = \{1824\lambda^2+(3360-115k)\lambda-100\,k+1536\}$$

$$h4_{4,0} = -4(\lambda+1)(152\lambda+9k+128) \tag{B3}$$

$$h1_{2,2} = 19\lambda^2+(92+16k)\lambda+64+4k$$

$$h2_{2,2} = -38\lambda^2-(184+36k)\lambda-128-24k \tag{B4}$$

$$h3_{2,2} = 19\lambda^2+(92+20k)\lambda+64+20k$$

and

$$h1_{4,4} = \{608\lambda^2+(1120-187k)\lambda+512-172k+20k^2\},$$

$$h2_{4,4} = \{-1824\lambda^2+(-3360+338k)\lambda-1536+308k-20k^2\},$$

$$h3_{4,4} = \{1824\lambda^2+(3360-115k)\lambda-100\,k+1536\},$$

$$h4_{4,4} = -4(\lambda+1)(152\lambda+9k+128). \tag{B5}$$

The constant coefficients in the expression of droplet shape as given in Eq. (36), are given by

$$\hat{L}_{2,2}^{(\mathrm{Ca})} = \frac{5}{48}\left(\frac{16+19\lambda-19\lambda\beta+4k\beta-16\beta}{-5\beta-5\lambda\beta+5\lambda+5+k\beta}\right). \tag{B6}$$

$$L_{2,0}^{(\mathrm{Ca}^2)} = \frac{\left\{\begin{array}{l}\left(a_0^{(20)}\lambda^3+a_1^{(20)}\lambda^2+a_2^{(20)}\lambda+a_3^{(20)}\right)\beta^3+\left(b_0^{(20)}\lambda^3+b_1^{(20)}\lambda^2+b_2^{(20)}\lambda+b_3^{(20)}\right)\beta^2\\ \quad+\left(c_0^{(20)}\lambda^3+c_1^{(20)}\lambda^2+c_2^{(20)}\lambda+c_3^{(20)}\right)\beta-25(19\lambda+16)(601\lambda^2+893\lambda+256)\end{array}\right\}}{1344(-5\beta-5\beta\lambda+\beta k+5+5\lambda)^3},$$

$$L_{2,2}^{(\mathrm{Ca}^2)} = \frac{\left\{\begin{array}{l}\left(b_0^{(22)}\lambda^3+b_1^{(22)}\lambda^2+b_2^{(22)}\lambda+b_3^{(22)}\right)\beta^2\\ \quad+\left(c_0^{(22)}\lambda^3+c_1^{(22)}\lambda^2+c_2^{(22)}\lambda+c_3^{(22)}\right)\beta+15(2\lambda+3)(16+19\lambda)^2\end{array}\right\}}{1152(-5\beta-5\beta\lambda+\beta k+5+5\lambda)^2},$$

$$L_{4,0}^{(\mathrm{Ca}^2)} = \frac{\left\{\begin{array}{l}\left(a_0^{(40)}\lambda^3+a_1^{(40)}\lambda^2+a_2^{(40)}\lambda+a_3^{(40)}\right)\beta^3+\left(b_0^{(40)}\lambda^3+b_1^{(40)}\lambda^2+b_2^{(40)}\lambda+b_3^{(40)}\right)\beta^2\\ \quad+\left(c_0^{(40)}\lambda^3+c_1^{(40)}\lambda^2+c_2^{(40)}\lambda+c_3^{(40)}\right)\beta+5(751\lambda+656)(19\lambda+16)(\lambda+1)\end{array}\right\}}{1344(-5\beta-5\beta\lambda+\beta k+5+5\lambda)^2(\beta k-9\beta-9\beta\lambda+9\lambda+9)},$$

$$L_{4,4}^{(\mathrm{Ca}^2)} = \frac{\left\{\begin{array}{l}\left(a_0^{(44)}\lambda^3+a_1^{(44)}\lambda^2+a_2^{(44)}\lambda+a_3^{(44)}\right)\beta^3+\left(b_0^{(44)}\lambda^3+b_1^{(44)}\lambda^2+b_2^{(44)}\lambda+b_3^{(44)}\right)\beta^2\\ \quad+\left(c_0^{(44)}\lambda^3+c_1^{(44)}\lambda^2+c_2^{(44)}\lambda+c_3^{(44)}\right)\beta-5(751\lambda+656)(19\lambda+16)(\lambda+1)\end{array}\right\}}{32256(-5\beta-5\beta\lambda+\beta k+5+5\lambda)^2(\beta k-9\beta-9\beta\lambda+9\lambda+9)}, \tag{B7}$$

where the constants in the above Eqs. (B6) and (B7) are given below:

$$\begin{aligned}
&a_0^{(20)} = 285475, \quad a_1^{(20)} = (664575-174100k),\\
&a_2^{(20)} = (5300k^2+478800-270800k), \quad a_3^{(20)} = 27200k^2-2400k^3-97600k+102400,\\
&b_0^{(20)} = -856425, \quad b_1^{(20)} = (-1993725+348200k),\\
&b_2^{(20)} = (541600k-1436400-35200k^2), \quad b_3^{(20)} = -26800k^2-307200+195200k,\\
&c_0^{(20)} = 856425, \quad c_1^{(20)} = (-174100k+1993725),\\
&c_2^{(20)} = (1436400-100k^2-270800k), \quad c_3^{(20)} = -400k^2+307200-97600k,
\end{aligned} \tag{B8}$$

$$\begin{aligned}
&b_0^{(22)} = 10830, \quad b_1^{(22)} = (-4465k+34485),\\
&b_2^{(22)} = (35040+440k^2-10220k), \quad b_3^{(22)} = 560k^2+11520-5440k,\\
&c_0^{(22)} = -856425, \quad c_1^{(22)} = (174100k-1993725),\\
&c_2^{(22)} = (-1436400+100k^2+270800k), \quad c_3^{(22)} = -307200+97600k+400k^2,
\end{aligned} \tag{B9}$$

$$
\begin{aligned}
&a_0^{(40)} = -71345, \quad a_1^{(40)} = (-193745 + 38200k),\\
&a_2^{(40)} = (-174880 + 69700k - 6570k^2), \quad a_3^{(40)} = 31680k - 52480 + 360k^3 - 6040k,\\
&b_0^{(40)} = 214035, \quad b_1^{(40)} = (-76400k + 581235),\\
&b_2^{(40)} = (6550k^2 - 139400k + 524640), \quad b_3^{(40)} = -63360k + 6000k^2 + 157440,\\
&c_0^{(40)} = -214035, \quad c_1^{(40)} = (38200k - 581235),\\
&c_2^{(40)} = (69700k - 524640 + 20k^2), \quad c_3^{(40)} = -157440 + 31680k + 40k^2,
\end{aligned} \tag{B10}
$$

and

$$
\begin{aligned}
&a_0^{(44)} = 71345, \quad a_1^{(44)} = (193745 - 38200k),\\
&a_2^{(44)} = (6570k^2 + 174880 - 69700k), \quad a_3^{(44)} = -31680k - 360k^3 + 6040k^2 + 52480,\\
&b_0^{(44)} = -214035, \quad b_1^{(44)} = (76400k - 581235),\\
&b_2^{(44)} = (-6550k^2 + 139400k - 524640), \quad b_3^{(44)} = -157440 + 63360k - 6000k^2,\\
&c_0^{(44)} = 214035, \quad c_1^{(44)} = (581235 - 38200k),\\
&c_2^{(44)} = (524640 - 69700k - 20k^2), \quad c_3^{(44)} = 157440 - 31680k - 40k^2.
\end{aligned} \tag{B11}
$$

The velocity fields in both the phases is written as

$$
\begin{aligned}
\mathbf{u}_{i,0} = \Bigg[& \frac{15}{4}\left\{\frac{r(1-\beta)(-1+r^2)}{-5\beta-5\lambda\beta+5+5\lambda+k\beta}\right\}\sin(2\phi)\sin(\theta)^2\mathbf{e}_r\\
&+\frac{5}{8}\left\{\frac{r(1-\beta)(-3+5r^2)}{-5\beta-5\lambda\beta+5+5\lambda+k\beta}\right\}\sin(2\phi)\sin(2\theta)\mathbf{e}_\theta\\
&-\frac{1}{4}\frac{r\left\{\begin{array}{l}-10\beta-10\lambda\beta+10+10\lambda+2k\beta\\ \quad -15\cos(2\phi)\beta+15\cos(2\phi)+25r^2\cos(2\phi)\beta-25r^2\cos(2\phi)\end{array}\right\}}{-5\beta-5\lambda\beta+5+5\lambda+k\beta}\sin(\theta)\mathbf{e}_\varphi\Bigg],
\end{aligned} \tag{B12}
$$

$$
\begin{aligned}
\mathbf{u}_{e,0} = \Bigg[& \Bigg\{-\frac{5}{4r^4}\frac{\left((-5\lambda+k-2)r^2+3\lambda-\frac{3}{5}k\right)\beta+(5\lambda+2)r^2-3\lambda}{(-5-5\lambda+k)\beta+5+5\lambda}\sin(2\phi)\sin(\theta)^2\\
&+\frac{r}{2}\sin(\theta)^2\sin(2\phi)\Bigg\}\mathbf{e}_r-\Bigg(\frac{1}{4r^4}\frac{(-5\lambda+k)\beta+5\lambda}{(-5-5\lambda+k)\beta+5+5\lambda}\sin(2\theta)\sin(2\phi)\\
&+\frac{r}{4}\sin(2\theta)\sin(2\phi)\Bigg)\mathbf{e}_\theta-\Bigg(\frac{1}{2r^4}\frac{(-5\lambda+k)\beta+5\lambda}{(-5-5\lambda+k)\beta+5+5\lambda}\sin(\theta)\cos(2\phi)\\
&-r\sin(\theta)\sin(\phi)^2\Bigg)\mathbf{e}_\varphi\Bigg].
\end{aligned} \tag{B13}
$$

The corresponding pressure field is given below

$$p_{i,0} = \frac{105r^2\lambda(1-\beta)}{(-20-20\lambda+4k)\beta+20+20\lambda}\sin(2\phi)\sin(\theta)^2,$$

$$p_{e,0} = -\frac{5}{2r^3}\left\{\frac{(-5\lambda+k-2)\beta+5\lambda+2}{(-5-5\lambda+k)\beta+5+5\lambda}\right\}\sin(2\phi)\sin(\theta)^2. \tag{B14}$$

APPENDIX C: EXPRESSION OF THE CONSTANTS PRESENT IN EQS. (43) AND (45)

The constants present in the expression of effective extensional viscosity in Eq. (43), are given by

$$\begin{aligned}
&m_0^{(1)} = -475, \quad m_1^{(1)} = (-1179+290k),\\
&m_2^{(1)} = (-732-59k^2+476k), \quad m_3^{(1)} = (-64+144k+4k^3-44k^2),\\
&m_0^{(2)} = -214035, \quad m_1^{(2)} = (76400k-581235),\\
&m_2^{(2)} = (-6550k^2+139400k-524640), \quad m_3^{(2)} = -157440+63360k-6000k^2,\\
&m_0^{(3)} = 214035, \quad m_1^{(3)} = (581235-38200k),\\
&m_2^{(3)} = (524640-69700k-20k^2), \quad m_3^{(3)} = 157440-31680k-40k^2.
\end{aligned} \tag{C1}$$

The constants present in the expression of N_1 and N_2 in Eq. (45) are given below:

$$\begin{aligned}
&n_{1,0}^{(1)} = 361, \quad n_{1,1}^{(1)} = (-152k+608), \quad n_{1,2}^{(1)} = (256+12k^2-128k)\\
&n_{2,0}^{(1)} = -722, \quad n_{2,1}^{(1)} = (152k-1216), \quad n_{2,2}^{(1)} = -512+4k^2+128k
\end{aligned} \tag{C2}$$

$$\begin{aligned}
&n_{1,0}^{(2)} = -5510, \quad n_{1,1}^{(2)} = (-16230+3497k),\\
&n_{1,2}^{(2)} = (-599k^2-19260+6916k), \quad n_{1,3}^{(2)} = -656k^2-8000+4112k+24k^3,\\
&n_{2,0}^{(2)} = 16530, \quad n_{2,1}^{(2)} = (48690-6994k),\\
&n_{2,2}^{(2)} = (57780-13832k+459k^2), \quad n_{2,3}^{(2)} = -8224k+576k^2+24000+28k^3,\\
&n_{3,0}^{(2)} = -16530, \quad n_{3,1}^{(2)} = (-48690+3497k),\\
&n_{3,2}^{(2)} = (-57780+140k^2+6916k), \quad n_{3,3}^{(2)} = -24000+4112k+80k^2.
\end{aligned} \tag{C3}$$

[1] M. Dressler and B. J. Edwards, Rheology of polymer blends with matrix-phase viscoelasticity and a narrow droplet size distribution, J. Nonnewton. Fluid Mech. **120**, 189 (2004).

[2] M. Dressler and B. J. Edwards, The influence of matrix viscoelasticity on the rheology of polymer blends, Rheol. Acta **43**, 257 (2004).

[3] H. A. Barnes, Rheology of emulsions - a review, Colloids Surfaces A Physicochem. Eng. Asp. **91**, 89 (1994).

[4] F. Lequeux, Emulsion rheology, Curr. Opin. Colloid Interface Sci. **3**, 408 (1998).

[5] P. Van Puyvelde, S. Velankar, and P. Moldenaers, Rheology and morphology of compatibilized polymer blends, Curr. Opin. Colloid Interface Sci. **6**, 457 (2001).
[6] C. L. Tucker III and P. Moldenaers, Microstructural evolution in polymer blends, Annu. Rev. Fluid Mech. **34**, 177 (2002).
[7] P. Fischer and P. Erni, Emulsion drops in external flow fields—The role of liquid interfaces, Curr. Opin. Colloid Interface Sci. **12**, 196 (2007).
[8] C. N. Baroud, F. Gallaire, and R. Dangla, Dynamics of microfluidic droplets, Lab Chip **10**, 2032 (2010).
[9] R. Seemann, M. Brinkmann, T. Pfohl, and S. Herminghaus, Droplet based microfluidics, Rep. Prog. Phys. **75**, 016601 (2012).
[10] H. A. Stone, A. D. Stroock, and A. Ajdari, Engineering flows in small devices: Microfluidics toward a lab-on-a-chip, Annu. Rev. Fluid Mech. **36**, 381 (2004).
[11] S.-Y. Teh, R. Lin, L.-H. Hung, and A. P. Lee, Droplet microfluidics, Lab Chip **8**, 198 (2008).
[12] A. Huebner, S. Sharma, M. Srisa-Art, F. Hollfelder, J. B. Edel, and A. J. Demello, Microdroplets: A sea of applications? Lab Chip **8**, 1244 (2008).
[13] D. Di Carlo, D. Irimia, R. G. Tompkins, and M. Toner, Continuous inertial focusing, ordering, and separation of particles in microchannels, Proc. Natl. Acad. Sci. USA **104**, 18892 (2007).
[14] Y. Zhu and Q. Fang, Analytical detection techniques for droplet microfluidics—A review, Anal. Chim. Acta **787**, 24 (2013).
[15] G. I. Taylor, The viscosity of a fluid containing small drops of another fluid, Proc. R. Soc. A Math. Phys. Eng. Sci. **138**, 41 (1932).
[16] G. I. Taylor, The formation of emulsions in definable fields of flow, Proc. R. Soc. A Math. Phys. Eng. Sci. **146**, 501 (1934).
[17] H. A. Stone, Dynamics of drop deformation and breakup in viscous fluids, Annu. Rev. Fluid Mech. **26**, 65 (1994).
[18] R. Pal, Fundamental rheology of disperse systems based on single-particle mechanics, Fluids **1**, 40 (2016).
[19] R. W. Flumerfelt, Effects of dynamic interfacial properties on drop deformation and orientation in shear and extensional flow fields, J. Colloid Interface Sci. **76**, 330 (1980).
[20] H. A. Stone and L. G. Leal, The effects of surfactants on drop deformation and breakup, J. Fluid Mech. **220**, 161 (1990).
[21] S. Velankar, P. Van Puyvelde, J. Mewis, and P. Moldenaers, Effect of compatibilization on the breakup of polymeric drops in shear flow, J. Rheol. **45**, 1007 (2001).
[22] Y. T. Hu and A. Lips, Estimating Surfactant Surface Coverage and Decomposing its Effect on Drop Deformation, Phys. Rev. Lett. **91**, 044501 (2003).
[23] H. K. Jeon and C. W. Macosko, Visualization of block copolymer distribution on a sheared drop, Polymer (Guildf). **44**, 5381 (2003).
[24] S. Velankar, H. Zhou, H. K. Jeon, and C. W. Macosko, CFD evaluation of drop retraction methods for the measurement of interfacial tension of surfactant-laden drops, J. Colloid Interface Sci. **272**, 172 (2004).
[25] S. Velankar, P. Van Puyvelde, J. Mewis, P. Moldenaers, S. Velankar, P. Van Puyvelde, J. Mewis, and P. Moldenaers, Steady-shear rheological properties of model compatibilized blends, J. Rheol. **48**, 725 (2004).
[26] W. J. Milliken, H. A. Stone, and L. G. Leal, The effect of surfactant on the transient motion of Newtonian drops, Phys. Fluids **5**, 69 (1993).
[27] P. M. Vlahovska, J. Bławzdziewicz, and M. Loewenberg, Small-deformation theory for a surfactant-covered drop in linear flows, J. Fluid Mech. **624**, 293 (2009).
[28] X. Li and C. Pozrikidis, The effect of surfactants on drop deformation and on the rheology of dilute emulsions in Stokes flow, J. Fluid Mech. **341**, 165 (1997).
[29] S. Yon and C. Pozrikidis, A finite-volume/boundary-element method for flow past interfaces in the presence of surfactants, with application to shear flow past a viscous drop, Comput. Fluids **27**, 879 (1998).
[30] E. Yariv and Y. Almog, The effect of surface-charge convection on the settling velocity of spherical drops in a uniform electric field, J. Fluid Mech. **797**, 536 (2016).
[31] M. Zabarankin, Analytical solution for spheroidal drop under axisymmetric linearized boundary conditions, SIAM J. Appl. Math. **76**, 1606 (2016).

[32] J. A. Lanauze, L. M. Walker, and A. S. Khair, The influence of inertia and charge relaxation on electrohydrodynamic drop deformation, Phys. Fluids **25**, 112101 (2013).
[33] M. Zabarankin, Liquid toroidal drop under uniform electric field, Proc. R. Soc. A Math. Phys. Eng. Sci. **473**, 20160633 (2017).
[34] J. Blawzdziewicz, P. Vlahovska, M. Loewenberg, J. Bławzdziewicz, P. Vlahovska, M. Loewenberg, J. Blawzdziewicz, M. Loewenberg, P. Vlahovska, and M. Loewenberg, Rheology of a dilute emulsion of surfactant-covered spherical drops, Phys. A Stat. Mech. Appl. **276**, 50 (2002).
[35] P. Vlahovska, J. Blawzdziewicz, and M. Loewenberg, Nonlinear rheology of a dilute emulsion of surfactant-covered spherical drops in time-dependent flows, J. Fluid Mech. **463**, 1 (2002).
[36] P. M. Vlahovska, On the rheology of a dilute emulsion in a uniform electric field, J. Fluid Mech. **670**, 481 (2011).
[37] K. Feigl, D. Megias-Alguacil, P. Fischer, and E. J. Windhab, Simulation and experiments of droplet deformation and orientation in simple shear flow with surfactants, Chem. Eng. Sci. **62**, 3242 (2007).
[38] P. C.-H. Chan and L. G. Leal, The motion of a deformable drop in a second-order fluid, J. Fluid Mech. **92**, 131 (1979).
[39] G. Hetsroni and S. Haber, The flow in and around a droplet or bubble submerged in an unbound arbitrary velocity field, Rheol. Acta **9**, 488 (1970).
[40] L. G. Leal, *Advanced Transport Phenomena* (Cambridge University Press, Cambridge, 2007).
[41] S. Mandal, A. Bandopadhyay, and S. Chakraborty, Effect of interfacial slip on the cross-stream migration of a drop in an unbounded Poiseuille flow, Phys. Rev. E **92**, 023002 (2015).
[42] J. Lee and C. Pozrikidis, Effect of surfactants on the deformation of drops and bubbles in Navier-Stokes flow, Comput. Fluids **35**, 43 (2006).
[43] S. Das, S. Mandal, S. K. Som, and S. Chakraborty, Migration of a surfactant-laden droplet in nonisothermal Poiseuille flow, Phys. Fluids **29**, 012002 (2017).
[44] G. K. Batchelor and J. T. Green, The determination of the bulk stress in a suspension of spherical particles to order c^2, J. Fluid Mech. **56**, 401 (1972).
[45] B. J. Bentley and L. G. Leal, An experimental investigation of drop deformation and breakup in steady, two-dimensional linear flows, J. Fluid Mech. **167**, 241 (1986).
[46] H. S. Kim and R. S. Subramanian, The thermocapillary migration of a droplet with insoluble surfactant: II. General case, J. Colloid Interface Sci. **130**, 112 (1989).
[47] A. Ramachandran and L. G. Leal, The effect of interfacial slip on the rheology of a dilute emulsion of drops for small capillary numbers, J. Rheol. **56**, 1555 (2012).
[48] W. R. Schowalter, C. E. Chaffey, and H. Brenner, Rheological behavior of a dilute emulsion, J. Colloid Interface Sci. **26**, 152 (1968).
[49] See Supplemental Material at http://link.aps.org/supplemental/10.1103/PhysRevFluids.2.113604 for the details on the boundary conditions and governing equations and the asymptotic analysis.